Universitetet i Stavanger

FACULTY OF SCIENCE AND TECHNOLOGY

MASTER'S THESIS

Study programme/specialisation: Automation and signal processing	Spring / Autumn semester, 2018 Open/Confidential
Author: Sigurd Myklebust	Sigurd Myklebust (signature of author)
Programme coordinator: Kjersti Engan Supervisor(s): Kjersti Engan and Kathinka D. Kurz	
Title of master's thesis: Cerebral vessel segmentation in contrast CT images	
Credits: 30	
Keywords: Image processing, CT, vessel segmentation	Number of pages: 57 + supplemental material/other: matlab code. 7z Stavanger, 15-06/2018 date/year

Abstract

Patients with cerebral stroke symptoms are typically examined using CT scanning due to its availability and efficiency. If the stroke is suspected to be ischemic, a contrast agent is injected to increase the contrast in the brain. Several images are acquired as the contrast enters the brain. This accentuates the vessels and shows how the contrast distributes in the brain. This helps to locate the stroke and the tissue that is affected by it, i.e. if is in risk of getting or already is irreversibly damaged.

This thesis uses contrast CT images of 11 stroke patients. The images are registered, and methods to remove skull and find vessel segments are developed and evaluated. The skull is removed by using wavelet coefficient decomposition to detect edges, and then perform thresholding and watershed segmentation to isolate the brain. To detect the vessel segments, two methods are implemented. One uses adaptive thresholding and the other uses unsupervised clustering based on the features that are typical for vessel segments. Both the skull removal and the vessel segmentation have visually been shown to be promising.

Contents

ABSTRACT **2**

PREFACE **4**

1 INTRODUCTION **5**
1.1 MOTIVATION 5
1.2 OBJECTIVE 5
1.3 LIMITATIONS 5

2 BACKGROUND **6**
2.1 CEREBRAL STROKE 6
2.2 COMPUTED TOMOGRAPHY 7
2.2.1 Contrast CT *8*
2.3 SEGMENTATION – RELATED WORK 11
2.4 REGISTRATION – A BRIEF INTRODUCTION 11

3 DATA MATERIAL **13**

4 METHODS **16**
4.1 SEGMENTATION OF PARAMETRIC MAPS 16
4.2 SEGMENTATION OF CT IMAGES 18
4.2.1 Rearranging images and removing redundant data *18*
4.2.2 Image registration *19*
4.2.3 Skull removal *20*
4.2.4 Vessel segmentation *24*
4.3 IMPLEMENTATION 30

5 EXPERIMENTS AND RESULTS **31**
5.1 SEGMENT PARAMETRIC MAPS 31
5.2 REGISTRATION OF CT IMAGES 34
5.3 SKULL REMOVAL 39
5.3.1 Selection of wavelet *39*
5.3.2 Result of the skull removal *41*
5.4 SEGMENT ARTERIES AND VEINS IN CT IMAGES 42
5.4.1 Finding vessels in patient 01 ..... *42*
5.4.2 Finding vessels in patient 03 ..... *44*
5.4.3 Finding vessels in patient 05 ..... *45*
5.4.4 Finding vessels in patient 07 ..... *47*
5.4.5 Finding vessels in patient 09 ..... *48*
5.4.6 Finding vessels in patient 11 ..... *50*
5.4.7 Differentiating arterial and venous vessels *51*

6 DISCUSSION AND CONCLUSION **53**

7 REFERENCES **55**

ATTACHMENT A: MATLAB CODE **57**

Preface

With the submission of this thesis, I finally fulfill what has seemed as too many years of studying. It has been an interesting and challenging journey, where the arrival at the destination never was certain.

Thanks to my thesis supervisors for useful inputs on the way, and for providing data that were interesting to work with.

Thanks to G. for exhibiting apparently unlimited patience and motivating support throughout the semester.

1 Introduction

1.1 Motivation

One out of six Norwegians will experience cerebral stroke in their lifetime [1]. This is a dramatic event, as it is likely to result in either disability or death. The occurrence increases with age, but both children and young adults can be affected [2]. Approximately one third of the patients will die and one third will suffer from permanent disabilities, while the remaining part will recover with minor or none permanent injuries [3]. It is the main cause of disability and requiring residential care, the third most common cause of death in Norway [4] and the second most common cause worldwide [5]. Survivors may suffer from reduced movement or paralysis, memory disorder, speech problems, reduced vision, change in mental health, etc. [6]. 15 000 people in Norway are affected by this yearly [3], which means that there are around 40 cerebral strokes each day. In addition to changing the lives of the patients and their relatives, the costs for treatment and rehabilitation are expensive for the society.

Stroke patients admitted to Stavanger University Hospital (SUS) are examined with computed tomography to diagnose the type of stroke, its location and thereby apply the correct treatment.

1.2 Objective

The aim of this thesis is to segment regions of interest in CT images of stroke patients, with an emphasis on finding penumbra and infarct core in CT perfusion maps, and arteries and veins in contrast CT images.

1.3 Limitations

As the focus will lie on the image processing, complex pathological and physiological explanations will not be given. It will be written from a non-medical technologist's point of view, keeping the use of medical terminology at a minimum. When needed, the medical explanations will scratch the surface, but hopefully be in-depth enough to give an understanding of the phenomena. To get a better view on the many variations and aspects, further reading elsewhere is suggested.

Another limitation is the number of patients. Only data from 11 patients are examined in this thesis.

2 Background

2.1 Cerebral stroke

The brain's blood supply consists of arteries supplying oxygen-rich blood from the heart to the brain, and veins returning used blood from the brain to the heart [7].

A cerebral stroke occurs when the blood supply is somehow disrupted, which leads to death of brain cells [8]. This happens when one or several arteries located in the head or neck region for some reason are malfunctioning. The reason divides the strokes into two main categories seen in Figure 1, which both have different variations and subcategories. Correct diagnosis is crucial in terms of applying efficient treatment. As the nature of the two types is different, wrong diagnosis and treatment may be mortal.

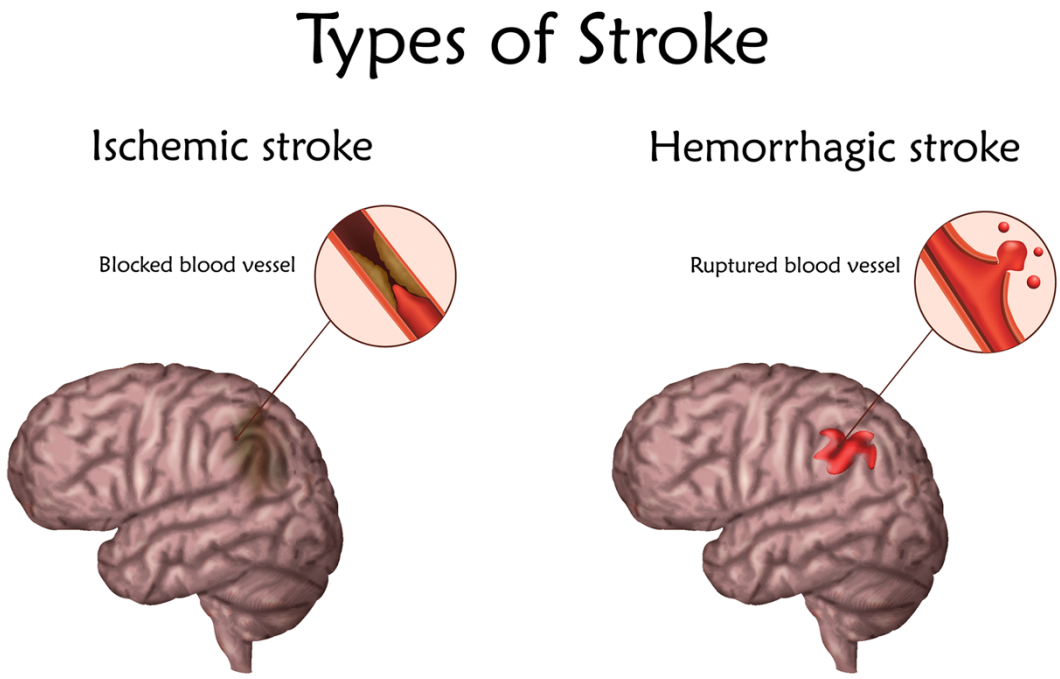

Figure 1: Types of stroke. Source: © maniki - stock.adobe.com. Reprinted using Standard Licence.

A stroke is classified as ischemic when it happens due to reduced or completely blocked blood supply, caused by a blood clot occluding an artery [8]. Responsible for 85-90% of the incidents [2], this is the most common type.

The affected region of an ischemic stroke is divided into infarct core and penumbra as seen in Figure 2, depending on the current state of the tissue. The infarct core consists of tissue being irreversibly damaged or dead due to lack of oxygen [9]. The penumbra is surrounding the core, and consists of tissue in risk of becoming permanently injured or dead [9]. Thus, it is still

salvageable if the oxygen supply is restored in time. If not, it will eventually transform to infarcted tissue.

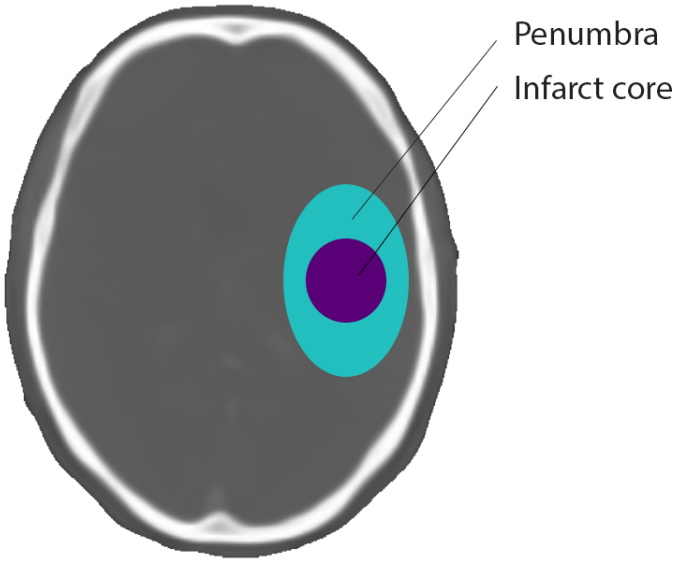

Figure 2: Illustration of penumbra and infarct core. The size and shape of both regions will vary.

If the stroke occurs due to bleeding, or more specifically an artery leaking blood into or around the brain, it is classified as hemorrhagic [8], applying to 10-15% of the incidents [2].

2.2 Computed tomography

The introduction of medical imaging is considered as a giant step, allowing visual inspections of the body's interior to be done non-invasive. The first commercial CT scanner was available in 1971 [10], and has evolved through the decades in terms of resolution, scanning time and other hardware related aspects [11]. Today, CT scans have a central role in investigating and diagnosing stroke patients correctly. Due to its availability and efficiency, patients with stroke symptoms are initially investigated with CT in many hospitals. The purpose of the investigation is to first determine if it is a stroke, determine the type, and eventually localize the infarction core, salvageable and dead tissue [12].

CT is derived from traditional x-ray; the images are acquired sending multiple x-rays through the organ being investigated [13]. The patient lies down with an x-ray generator and detectors placed in a cylinder around the body part that is examined. This is rotated around the organ, shooting x-rays from various angles $[0°,360°\rangle$. The intensity from the transmitter to the receiver is then reduced due to attenuation in the tissue [14].

The process can be explained by visualizing the x-ray as a straight line passing through a point with polar coordinates (ρ,θ) in a disk, where the disk is the organ. Mathematically, it is described in [14] as

$$I = I_0 e^{-R(\rho,\theta)},$$

where

$$R(\rho, \theta) = \int u(\rho \cos\theta - s \sin\theta\, , \rho \sin\theta + s \cos\theta)\, ds.$$

I denotes the detected intensity, I_0denotes the transmitted intensity, s is the distance from the line entering the organ to the point (ρ, θ) and $u(\rho, \theta)$ is the attenuation or optical density in the point [14]. By combining intensity measurements from multiple orientations and using a reconstruction algorithm, it is possible to reconstruct a 2D image or slice of the organ. If several 2D images are reconstructed from several positions, these can be stacked together to form a 3D image [13].

The CT images are saved as DICOM files, which is the standard format for storing medical images [15]. The files contain both pixel values and multiple lines of metadata. The latter consists of detailed information about the patient and the acquisition process. This includes patient information, body part examined, exposure time, x-ray tube current, and more. Detailed information about the metadata in a CT DICOM file can be found in [16].

The pixel values are typically 12 bits, which means there are 4096 possible intensity values. They are corresponding to the Hounsfield scale [17] with or without an offset and a scaling, also known as the rescale intercept and rescale slope [16]. Thus, the relationship between a HU value and pixel value is:

$$HU\ value\ = (rescale\ slope) * (pixel\ value)\ +\ rescale\ intercept,$$

as described in [18].

The Hounsfield unit is a measure of the attenuation of x-rays in a material, and is defined by arbitrarily setting the attenuation of air and water to be -1000 and 0 [17], respectively.

2.2.1 Contrast CT

A contrast agent is injected to get a better view of the cerebral circulation. When the agent is given, a CT scan is performed. Unlike non-contrast CT, multiple images of the same slices are acquired over a short time period. As seen in Figure 3, this shows how the agent and hence the blood distributes in the brain.

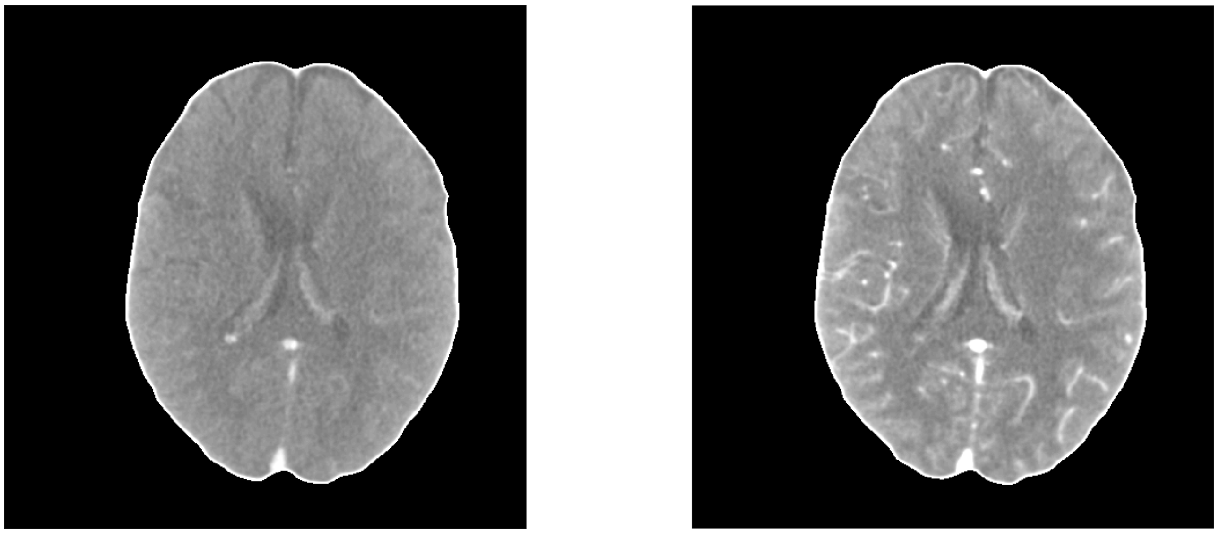

Figure 3: Same slice of the brain before and after contrast bolus arrives.

Since each slice of the brain consists of several two-dimensional images from different acquisition times, they can be thought of as three-dimensional images. The spatial information will then be in the x,y-plane, and the temporal information will be along the z-axis. Being in possession of time data in addition to the images, time-density curves are obtained. They show how the attenuation change as a function of time when the contrast medium flows through the brain, as seen in Figure 4. Such a curve exists for each pixel in each slice. If 30 512x512 pixel images are acquired of 15 slices and the brain occupies a third of the area, approximately 1.3M curves exist. They are the basis for the CT perfusion modality.

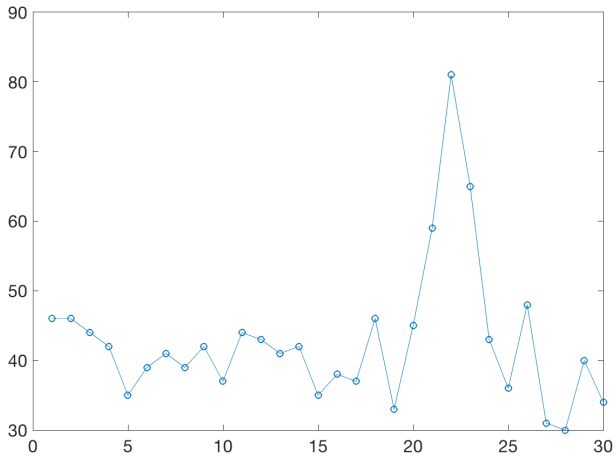

Figure 4: Time density curve: Attenuation in a pixel change over time as contrast medium is injected.

Maximum intensity projection (MIP) and minimum intensity projection (MinIP) seen in Figure 5 are useful visualizations of the temporal information available in a slice. They are two-dimensional grayscale images depicting the maximum and minimum pixel intensities for each pixel along the time-axis.

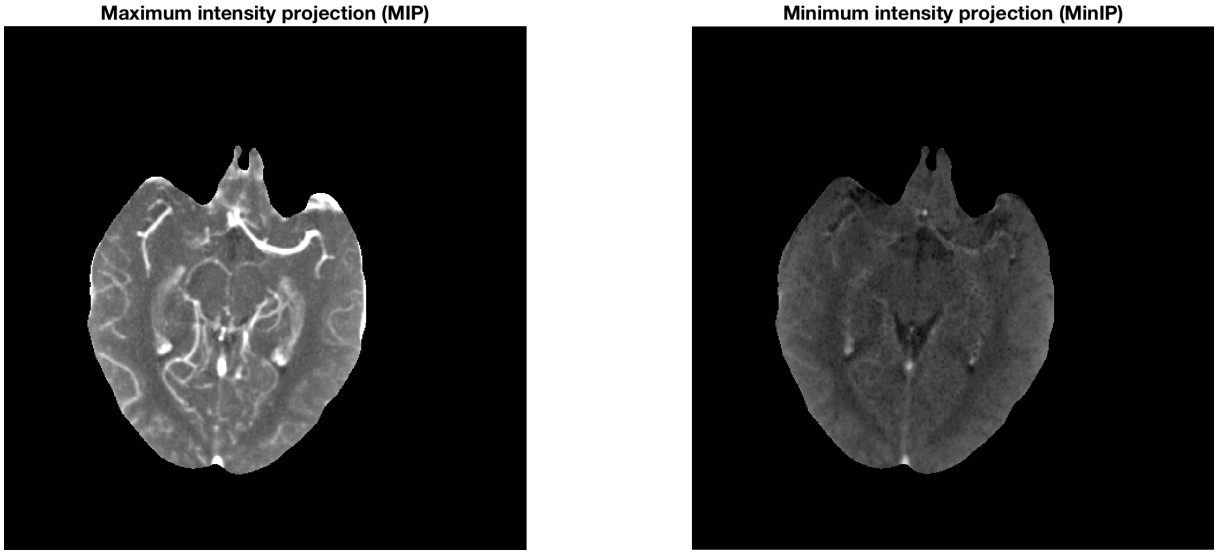

Figure 5: Maximum and minimum intensity projection. Display range: [1000 1200]

Other measures that can be derived are from the time-density curves are perfusion parameters. The simplest is the time to peak (TTP), which is the time from the contrast medium is given to the attenuation reaches its maximum. The other measures are found mathematically using either deconvolution or non-deconvolution-based methods [19] combining the time-density curves for the tissue, and an arterial and a venous input function. The most used commonly used measures in terms of stroke diagnosis in addition to the already established TTP, are the cerebral blood flow (CBF), cerebral blood volume (CBV) and the time-to-maximum of (TMAX) of the residue function as described in [20].

The resulting parameters are visualized as parametric color-coded maps as shown in Figure 6, indicating the values [19]. By convention, red indicates a high value, and blue/purple indicates a low value. In general, a normally perfused brain would have roughly symmetrical perfusion maps, with short TTP and TMAX, and high CBF and CBV [21].

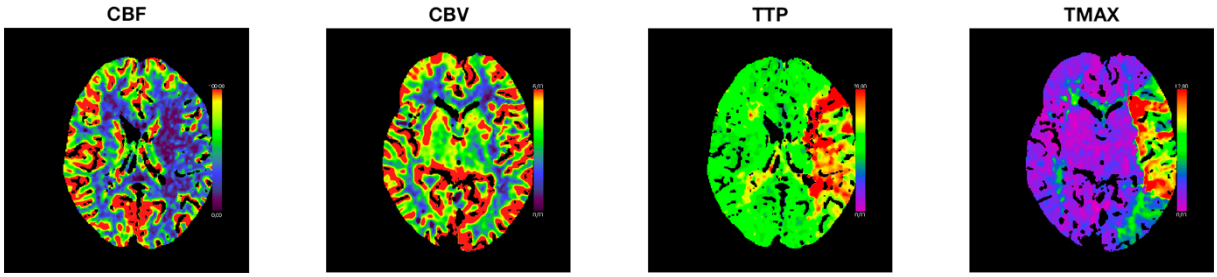

Figure 6: Parametric maps visualizing different parameters.

When interpreting these together, trained medical personnel are able to spot the perfusion abnormalities that may indicate a possible ischemic stroke. These are typically low CBF and CBV, and long TTP in a region. As Figure 6 shows, there is a notable asymmetry in the

perfusion; something is going on in the right[i] hemisphere. The maps indicate reduced CBF and CBV, and increased TTP in the same area, i.e. there is an ischemic stroke.

How to precisely classify core and penumbra in perfusion maps, is an ongoing discussion and research topic. The results in the studies are varying, as some present arguments for the use of one perfusion parameter alone, and others suggest combinations of these. Lin et al [22] describes the penumbra as a region with prolonged TTP/Tmax and normal to slightly decreased CBV/CBF, and the infarct core as a region with markedly increased TTP/Tmax and low CBV/CBF [22].

2.3 Segmentation – related work

Several techniques for general purpose image segmentation exist. There are written several in-depth reviews of these and more specific methods to segment blood vessels in different imaging modalities [23] [24].

Meijs et al. [25] suggest vessel segmentation using a Random Forests classifier [26] with in total 9 different features:

- The weighted[ii] temporal average image [25].
- The weighted temporal variance image [25].
- The Hessian eigenvalues [25].
- The first temporal image [25].
- The mean, mode, standard deviation and entropy of the weighted temporal variance [25].

One segmentation technique alone is often not enough to achieve an acceptable segmentation, so a combination of several are often used.

2.4 Registration – a brief introduction

Image registration tries to align different images acquired of the same object/scene onto each other [27]. The purpose is to make equal pixel coordinates correspond to the same spatial coordinates [27]. This is necessary if either the camera or the object, or both, have different positions in the acquisitions [27]. Another cause can be changes in the acquisition process, such as different equipment [27].

As described in [27], a registration procedure can typically be divided into four parts:

1. Extract features from the images.
2. Match features in the reference and the moving images.

i CT images depict the brain seen from below; the brain's directions are opposite to the directions in the image. The left hemisphere is in the right side of the image, and vice versa.

ii The weights are used due to different exposure settings in the different temporal images [24].

3. Estimate a geometric transformation to align the corresponding features.
4. Transform the images.

How the objects differ in the reference and the moving images, can be described by the distortion parameters. The most basic are the ones that preserve parallel lines, as seen in Figure 7.

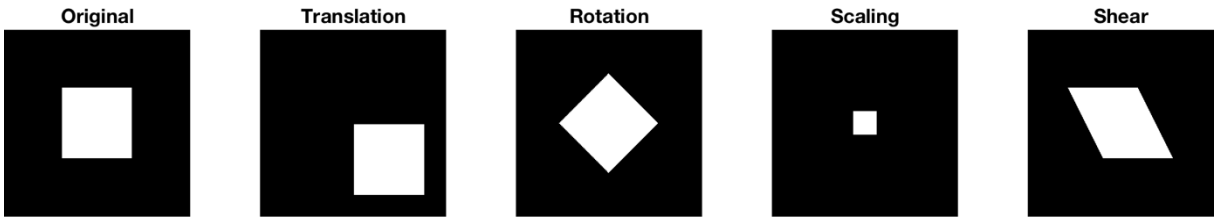

Figure 7: A visualization of how an image can be distorted.

3 Data material

The data material consists in total of 4620 contrast CT images and 160 parametric maps of 11 selected, anonymized patients admitted to SUS from 2014 to 2015. All are suffering from ischemic strokes located in one of the hemispheres. An overview of the dataset is given in Table 1. Some details about the acquisition processes are found in Table 2.

The perfusion images are 30 images acquired from each of the 13-22 slices with slice thickness 5 mm, as shown in Figure 8. This means there are 390-660 images for each patient. From these, parametric maps containing CBF, CBV, TTP and TMAX are generated for each slice. This gives 4x13-22 parametric maps for each patient.

- The CT images are grayscale or intensity images of size 512x512 with pixel values in the range [0,4095], with rescale intercept -1024 and rescale slope 1. Thus, a pixel value can be translated to a HU value by subtracting 1024 from it.
- The parametric maps are RGB images of size 512x512x3, with each channel having intensity values in the range [0,255].

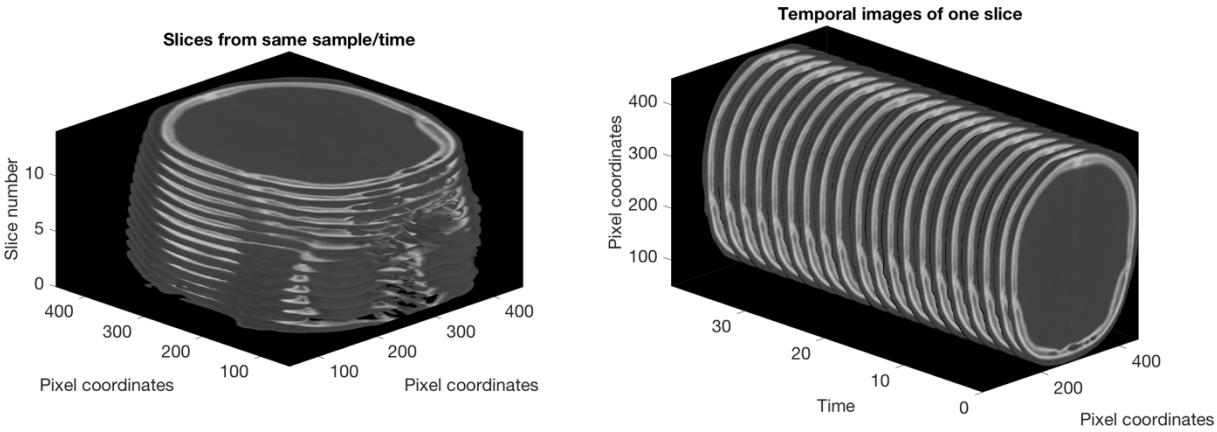

Figure 8: Left: 13 slices of the head. Right: Temporal images of one of the slices.

Patient	01	02	03	04	05	06	07	08	09	10	11
Age	64	56	67	69	65	77	87	70	63	67	83
Sex	M	F	F	M	M	F	F	M	F	F	M
Maps	19	13	13	13	13	13	13	13	22	14	14
Images	390	390	390	390	390	390	390	390	660	420	420
Slices	13	13	13	13	13	13	13	13	22	14	14

Table 1: Overview of the dataset.

Patients	01-08	09-11
Xray tube current	416	350
Exposure time	600	570
Exposure	250	200
kVp	80	80

Table 2: Exposure parameters.

As seen in Figure 9, the interval between the samples is shorter in the first half of the scan.

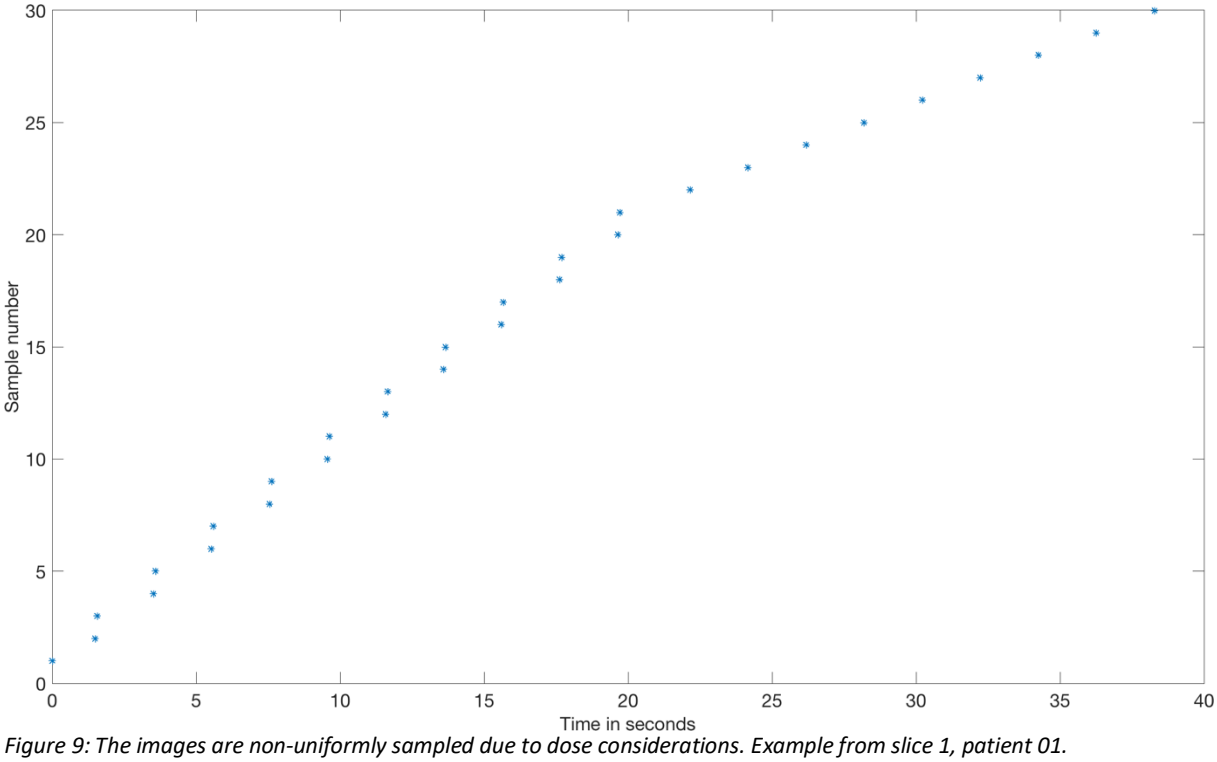

Figure 9: The images are non-uniformly sampled due to dose considerations. Example from slice 1, patient 01.

Before starting processing the CT images, it is necessary to look at how they are arranged. Their filenames consist of IM followed by six digits in the range from zero to the number of images - 1. For patient 01, the first and last images will then be IM000000 and IM000389, respectively. A natural assumption will be that they are sorted either by slice or acquisition time. When investigating the DICOM-headers containing information about the series of images, this is actually not the case.

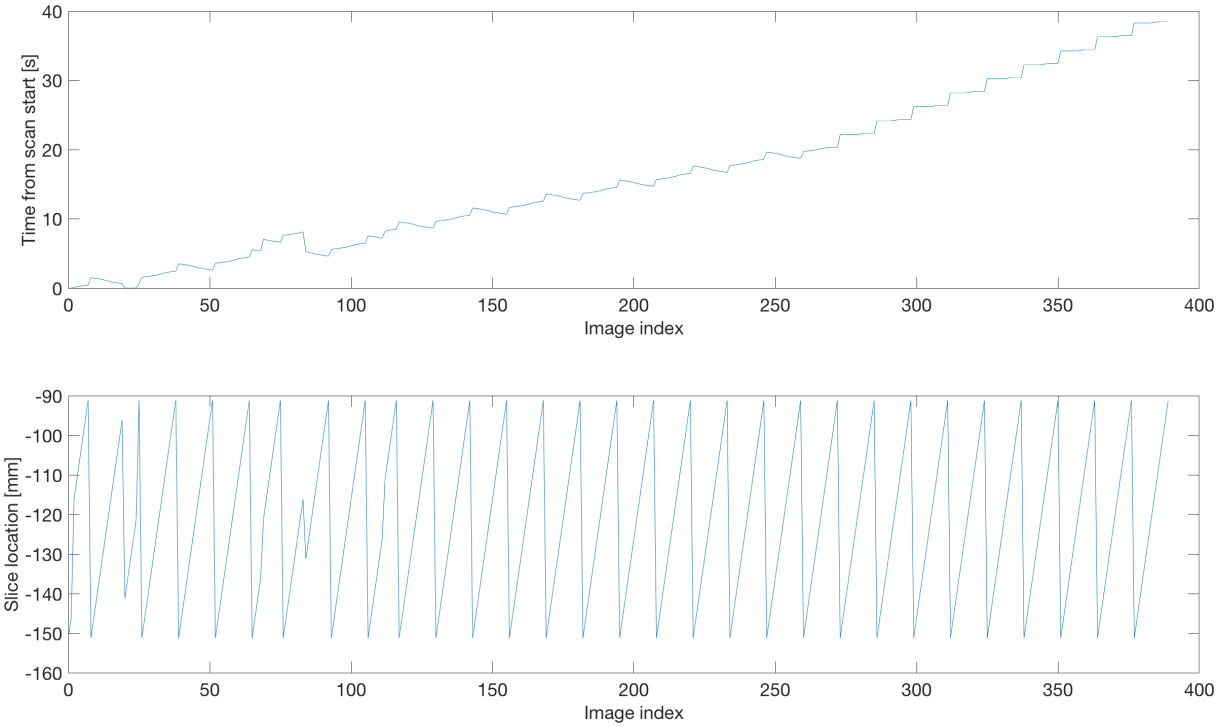

Figure 10: Comparing image index against time from scan start and slice location. Patient 01.

As seen in the figure, neither the slice location or time from scan start are strictly increasing functions of the image index or file number. Therefore, the images have to be rearranged.

4 Methods

4.1 Segmentation of parametric maps

To segment core and penumbra, the information available in the parametric maps is used. Since the metadata for the perfusion maps contain no information about how the pixel values and parametric values relates to each other, it is necessary to establish such a relationship. This is done by a simple manipulation of the information available in the image, as described in Algorithm 1.

Input: Parametric map. Color bar.

1. Assign a parametric value to each color in the bar, ranging from 0 to the max of the parameter range.
2. Find the unique colors in the map.
3. Compare the colors in the bar and in the map.
4. The bar is expanded with the colors that differs.
5. Convert the color bar to the HSV color space.
6. Sort the colors by hue, saturation and value.
7. Assign a parametric value to the added colors by averaging the parametric values below and above.
8. Convert the color bar back to RGB.

Output: Matrix containing the relationship between colors and parametric values.

Algorithm 1: Manipulation of the pixel information to establish a relationship between pixel values and parameter values when no such information is included in the metadata.

Each map contains a color bar depicting the range of the parameter as seen in Figure 11. The TMAX and the TTP maps have equal color bars, but with ranges $[0, 12]$ and $[0, 20]$, respectively. The CBF and CBV maps also have equal color bars, but with ranges $[0, 100]$ and $[0, 6]$, respectively. The bars have 256 unique colors, which gives 256 possible parametric values. Examples of RGB and HSV values in Table 3 demonstrate that the colors can be sorted by their HSV values.

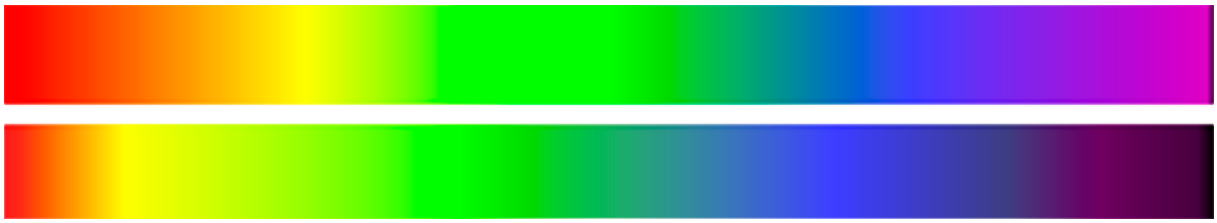

Figure 11: Top: Color bar for CBF and CBV. The ranges are [0, 100] and [0,6]. Bottom: Color bar for TTP and TMAX. The ranges are [0, 12] and [0, 20]. Values descend from left.

Index	Red	Green	Blue	Hue	Saturation	Value
0	254	0	0	0.00	1.00	1.00
85	169	254	0	0.22	1.00	1.00
170	42	128	168	0.55	0.75	0.66
255	95	0	95	0.83	1.00	0.37

Table 3: RGB values and corresponding HSV values rounded to the two nearest digits.

Some dissimilar color bands can occur in the extended bars, so the method is not flawless. Notice e.g. that there is a thin, dark line almost at the right edge of the extended bar which differs from the surrounding colors. Apart from this, the method seems to function reasonably when the original and extended bars are compared by visual inspection, as they look pretty similar.

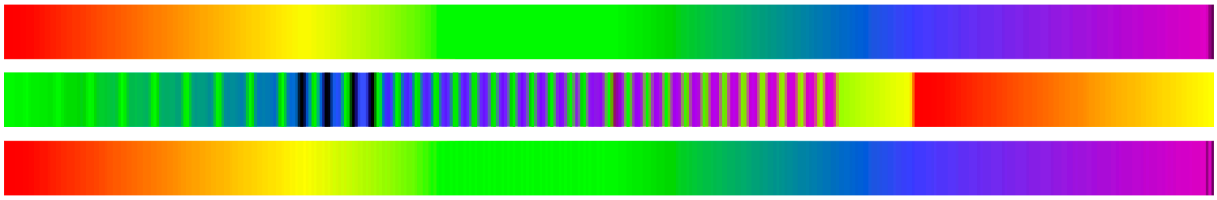

Figure 12: Top: Original color bar. Middle: Colors in a map that are not present in the color bar. Bottom: Expanded color bar.

All the colors have now been associated with a parametric value. Thus, the segmentation of the maps can be done by setting the parametric values that best define the regions of interests.

The hemisphere affected by the stroke is located by dividing the TMAX mask containing TMAX values above 6 into two halves, and then counting the number of pixels. The half with the largest number is the region of interest, and the other half is set to zero. Since all the patients have strokes located in one of the hemispheres alone, this can be done. The next step is to classify the tissue as either salvageable or irreversibly damaged, i.e. penumbra or infarct core. This is done by combining the TMAX mask and the CBF mask.

The CBF threshold defining infarct core is set to 30% of the mean CBF in the healthy hemisphere. When the infarct core in the ROI is found, the remaining tissue in the TMAX mask is classified as penumbra. I.e. the TMAX-CBF mismatch is used to determine the state of the tissue. Both the values and the parameters can be changed to see how this affects the penumbra and core estimates.

4.2 Segmentation of CT images

To find the vessels in the contrast-enhanced CT images, several processing steps are required. These are divided into four main parts, which each contains several sub-parts.

1. The images are rearranged, so that they are sorted in a logical fashion.
2. The images are registered to compensate for patient movement.
3. The skull and other uninteresting parts are removed.
4. The vessel segmentation is performed.

4.2.1 Rearranging images and removing redundant data

This method simply just rearranges the images, so that they are sorted temporally. For each image, acquisition time and slice location contained in the DICOM header are read. When this information is gathered for each patient, the images are sorted by slice and time, respectively. This preparation of the data is crucial, and is probably done by default in most of the commercially available software in the hospitals.

As an additional step, removal of redundant data is performed in the same method. Only the largest object that is brighter than 400, i.e. the head, is kept. This removes parts of the table being visible in some of the images, as seen in Figure 13. If it is not removed, it might degrade the performance of the registration, as the table is fixed, and the head is not. This also suppresses unwanted information present as low-intensity pixel values in the background. This is only visible when manipulating the display range for pixel intensities, as seen in Figure 14.

In addition, all pixel values below 800 are set to 0. This can be done since the brain typically has pixel values above 1000 [28].

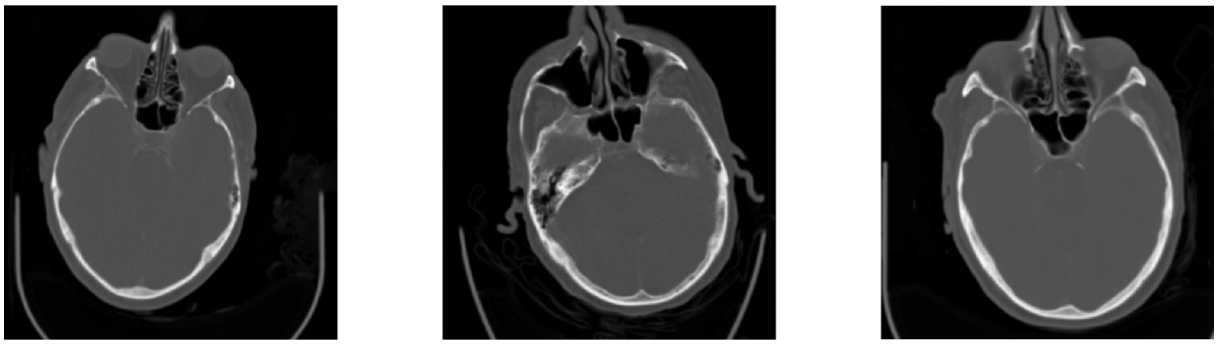

Figure 13: Parts of the table visible in some of the images.

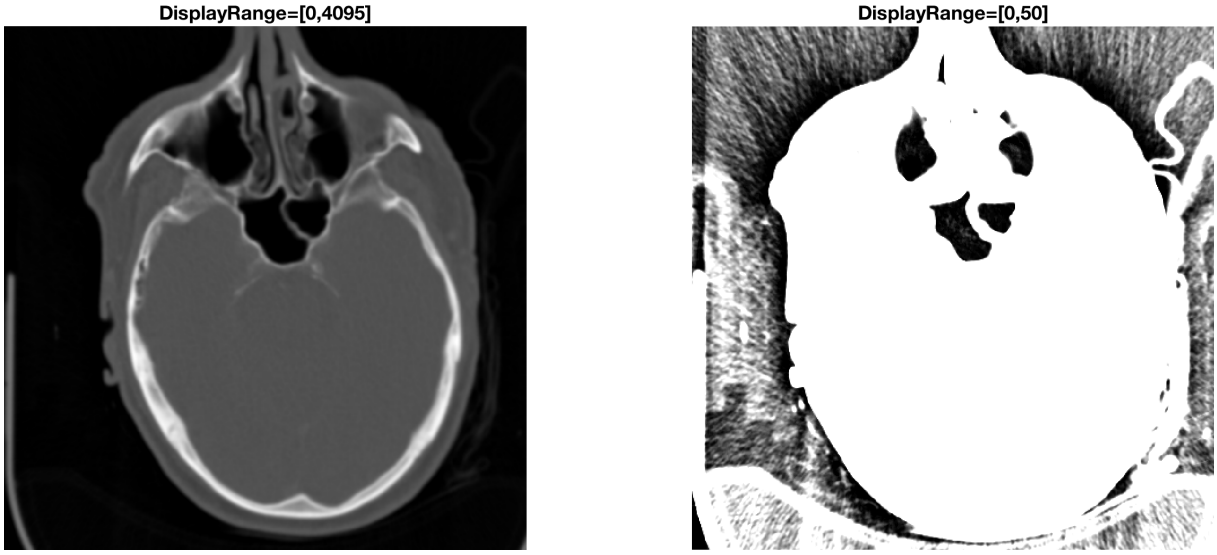

Figure 14: Left: Image displayed with its full intensity range. Right: Same image displayed with intensity range [0,50], meaning that all values from 50 and above will be interpreted as white. This reveals low-intensity noise in the background.

4.2.2 Image registration

To spatially align the images in each slice, the images are registered using the similarity transformation. Thus, translation, rotation and scaling will be compensated for. Two methods are evaluated, which use different optimizers and similarity metrics.

Input: All the images in a slice.

1. Reference = First image.
2. Moving = The remaining images.
3. For each of the moving images:
    a. Compute the phase correlation between the reference and the moving images to estimate an initial geometric transform.
    b. Use the initial geometric transform as a start, and iteratively find the geometric transform that optimizes the similarity metric.
    c. Align the moving image to the reference using the geometric transform.

End

Output: Images that are spatially aligned.

Algorithm 2: A description of the image registration.

The first temporal image in each slice is set as the fixed image, and the 29 remaining are registered against this. Both methods are iterative and use an optimizer to get the best similarity between the images. The registration is intensity-based but use phase correlation in addition to estimate an initial geometric transformation. The difference between the methods is the optimization algorithm and the similarity metric used.

In the first method, the images are treated as monomodal images. The regular step gradient descent algorithm minimizes the mean squared error between the fixed and the registered image. The second treats them as multimodal images. The one-plus-one evolutionary optimizer maximizes the mutual information contained in the fixed and the registered images. Both methods estimate an initial geometric transformation by computing the phase correlation described in [29].

The optimal optimization parameters can be found experimentally. Adjusting each of them individually and evaluate the result is time consuming. Instead, a simple approach can be to adjust the default parameters by the same scaling factor. This is done for the One-Plus-One Evolutionary optimizer as follows:

$$GrowthFactor = \frac{GrowthFactor - 1}{Scaling} + 1$$

$$Epsilon = \frac{Epsilon}{Scaling}$$

$$InitialRadius = \frac{InitialRadius}{Scaling}$$

$$MaximumIterations = MaximumIterations * Scaling.$$

The intensity levels of the skull are assumed to be constant during the scan, as it is unaffected by the bolus. Secondly, it is significantly brighter than the brain. Under these assumptions, a measure is to see how the skull is aligned in the images being registered. Logical arrays containing pixels brighter than 1900 are found for the reference, the moving and the registered images. The thought is that these will contain only the skull. These are then combined using an exclusive or operation, and then compared with respect to the number of ones. A low number of ones will then indicate a good registration. The means for the images are computed, which gives the error for each patient. This is used to evaluate the performance of the registration in addition to the traditional performance measures mutual information and mean squared error.

4.2.3 Skull removal

When the images are registered, the skull can be removed. To do this, it is necessary to state the features describing it.

- In contradiction to the brain, the skull is unaffected by the contrast bolus. Thus, its intensity values will not change over time, and can be assumed to be in a constant range. In addition, the skull is brighter than the rest.

- The skull is characterized by a sudden change in the brightness.

- The sudden change in brightness can also be thought of as high frequencies.

Based on these properties, at least three different methods to detect the skull can be derived.

1. The simplest will be to detect it by thresholding. A challenge here is the nature of the images. Since each image actually depicts a 5 mm thick slice, a potential problem is that bone can be partially occluded by tissue. It will then appear with a lower intensity value. Another possible problem is that the density of the bone may vary between the patients, and also from slice to slice. Thus, it is discarded.

2. When a change is apparent, it implies that the derivative and thus the gradient of the image contain useful information. A method is therefore to use traditional first- or second-order operators to detect the edges, which then will correspond to the skull.

3. The transition between the skull and the brain will correspond to a high frequency. Since the Fourier transform contains no information about their location, wavelets seem like a useful approach.

4.2.3.1 Edge detection with wavelets

The idea is that the edges can be characterized by another feature than their gradient, which is the frequencies. With these, the images are decomposed into detail and approximation coefficients. The high frequencies, i.e. the edges, will then be found in the detail coefficients, which are 3 matrices containing the vertical, horizontal and diagonal details.

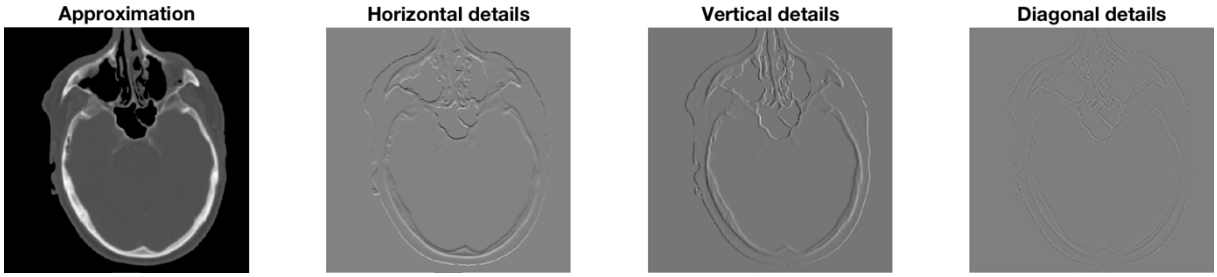

Figure 15: Example of decomposed coefficients.

As the figure shows, the skull is clearly visible in both the horizontal and vertical detail coefficients. There is also some information present in the diagonal coefficients, but this is hard to see. These results tell that the wavelet approach also will be able to detect the edges, like initially hypothesized.

In the given application, it is desirable to retain the dimensions of the original image. Thus, downsampling is both unwanted and unnecessary. This implies the selection of the discrete stationary wavelet transform. With a chosen wavelet and a given number of decomposition levels, the wavelet coefficients are found. As these can be either positive or negative, some sort of standardization is useful. A rescaling is done which maps the coefficients to positive integers in the range $[1,1000]$.

The edge detection is performed in the wavelet domain. This is done by thresholding the detail coefficient matrices by an appropriate value, either absolute or relative, and then combine

these by logical OR operators. The result will then be a binary mask with the edges, which ideally corresponds to the skull. This is then treated in a similar way as the mask in the previous subchapter. The al

Input: CT perfusion image, *Im*

1. [cH,cV,cD] = Horizontal, vertical and diagonal detail coefficients of Im.
2. [cH,cV,cD] = Rescale coeffcients to the range [1,1000].
3. T = 14, threshold value found by trial and error.
4. EdgeMask = cH>T OR cV>T OR cD>T

Output: Binary image, *EdgeMask*

Algorithm 3: Algorithm to detect edges using wavelets.

4.2.3.2 Processing the edge masks

For the first temporal image in each slice, the skull and other unwanted parts are removed. This gives a mask which isolates the brain. The resulting mask can then be applied to the remaining 29 images in the slice, since these are registered against the first. To get this mask, several processing steps are performed on the binary mask containing the edges found either by traditional edge detection or wavelets.

The second part of the algorithm consists of some simple operations performed on the edge mask to prepare it for the next steps. The objects are filtered by area, so that only the largest objects in the mask are kept. These are then filtered with a Gaussian filter to give smoother boundaries, and at last their holes are filled.

The third part consists of segmenting the mask found in the previous part. When the brain appears as a fairly round object surrounded by a dense and coherent skull, which typically is the case in the upper slices, the previous part alone is enough to isolate it. In the lower slices it gets more challenging. The brain can then be separated into many different parts by the skull. In addition, there are other disturbing objects as well, i.e. the eyes and more, as seen in Figure 16. It is necessary to distinguish between these.

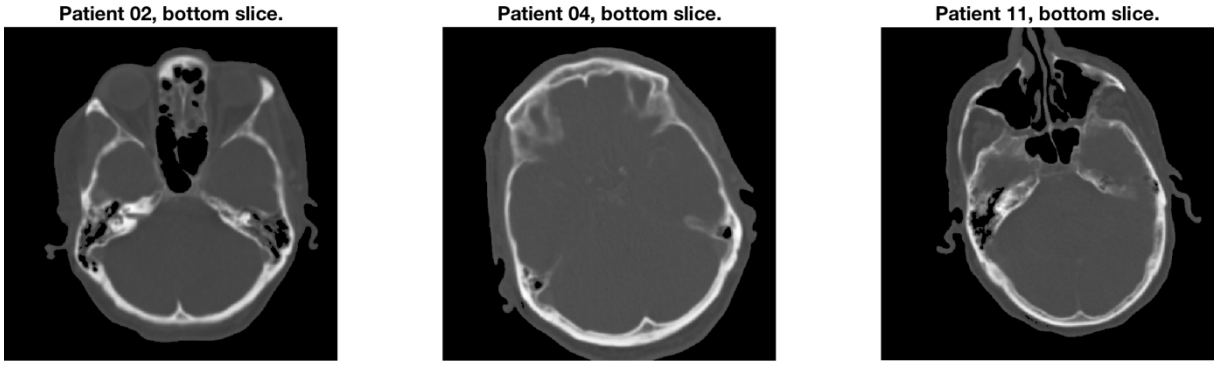

Figure 16: The skull is not a coherent, ellipsoid-like edge in the lower slices.

The transition between the eyes and the brain are often seen as a narrow passage. The idea is to differentiate these from each other by using Watershed segmentation. The eyes will then make one catchment basin each, and the brain another, which are separated by the narrow transition which will correspond to the ridge line. The steps in Algorithm 4 are from the method outlined in [30].

Input: Binary image, *EdgeMask*

1. D = Compute the negative Euclidean distance transform of the inverse edge mask.
2. H_min = Compute the H-minima transform of D to remove the shallowest regions.
3. BW_min = Only the regional minima of H_min.
4. D = Impose BW_min on D.
5. L = Compute the Watershed transform of D.

Output: Label matrix, *L*

Algorithm 4: Algorithm to separate the brain from the rest.

When the different segments are found, they are analyzed by looking at their properties. This is the fourth part. The first property describing a region is the area. The largest region is assumed to be a part of the brain. For the remaining regions, the perimeter values and Euclidean distance to the largest region are computed. Using the perimeter value *P* and the area *A*, the circularity measurement defined as

$$C = \frac{4\pi A}{P^2}$$

in [31] for a region is computed. If either the area or the circularity value is too small, or the distance to the largest object is too large, the region is removed. The binary mask will now contain ones where the brain is located. When the input image is multiplied by the mask, the output will be an image only containing the brain. The algorithm is shown in Algorithm 5.

Input: Label matrix, *L*

1. A = Compute area of all the regions in L.

2. For all except the largest region:
   P = Perimeter of the region.

   CF = Circularity factor of the region.

   Dist = Euclidean distance between the region and the largest region.

   If cf<0.45 OR Dist>170 OR A<500
      Remove region.
   End
   End

3. BW = Binary mask with all regions.

Output: Binary mask, *BW*.

Algorithm 5: Algorithm for removing objects that are not a part of the brain.

A walkthrough of the skull removal is shown in Figure 17.

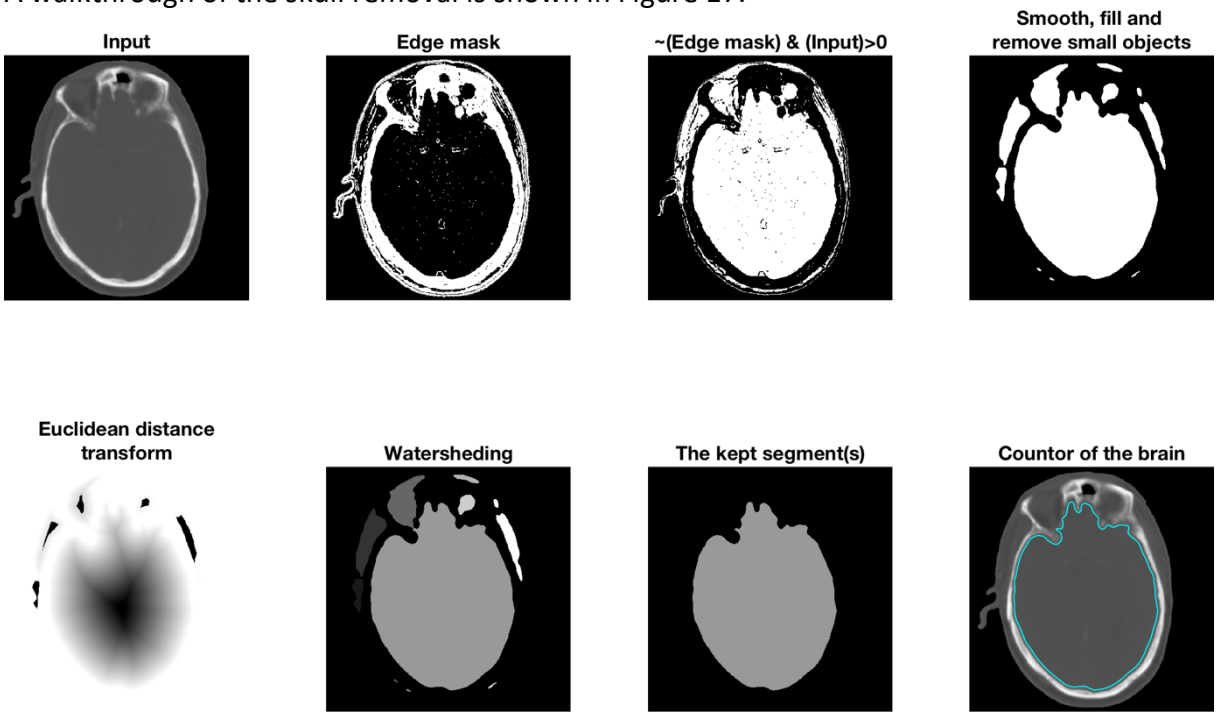

Figure 17: A visualization of the different steps in the skull removal.

4.2.4 Vessel segmentation

4.2.4.1 Preprocessing

The background is completely black with intensity 0, while the brain typically has intensities above 1000. This gives a sharp transition between them. This can possibly lead to unwanted and unexpected behavior when applying different processing techniques to the images, e.g.

when smoothing. To avoid this, the zero elements, i.e. the background, are replaced by the mean of the non-zero elements, i.e. the foreground. This is demonstrated in Figure 18.

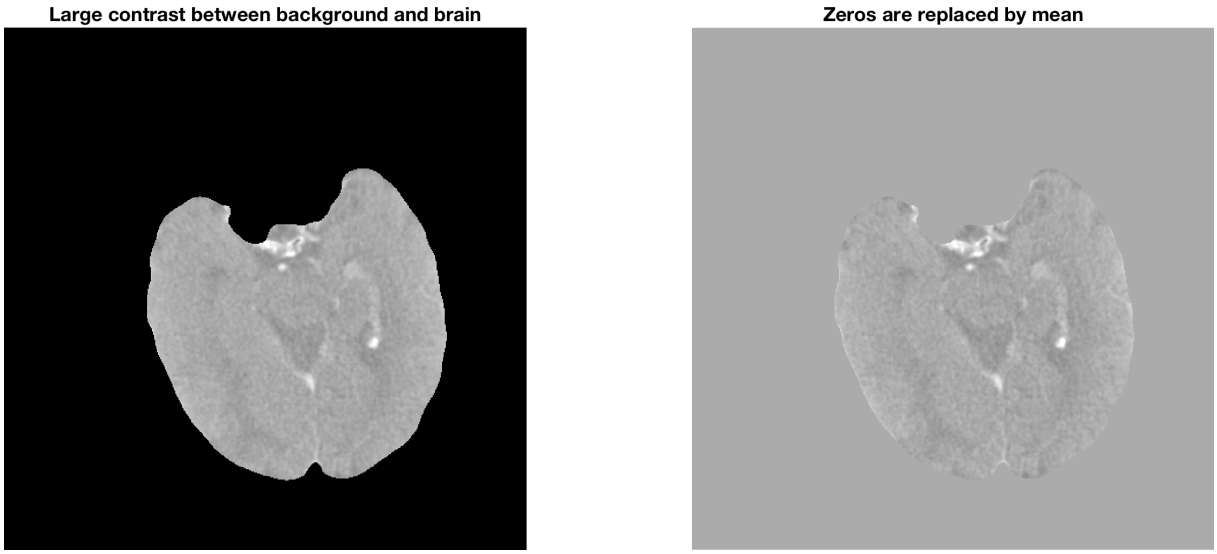

Figure 18: Replacing zeros by mean of non-zero elements to avoid sharp transition between brain and background.

To reduce the influence of noise and possible errors introduced in the registration, a smoothing is necessary. A simple 3D Gaussian smoothing filter specified with standard deviations

$$[\sigma_x \quad \sigma_y \quad \sigma_t] = [0.25 \quad 0.25 \quad 1]$$

and kernel size $3\ x\ 3\ x\ 5$ is applied to the images in each slice. Thus, the images are smoothed in both the spatial and temporal direction. These parameters have been chosen by visually inspecting the outcome. Other more sophisticated filters have not been taken into consideration, but can possibly yield a better result.

4.2.4.2 Segmentation using adaptive thresholding

To segment the vessels, the available temporal information has to be exploited. The idea is that the vessels will be found in the regions where the change in pixel intensities are most prominent. These are best visualized by looking at the MIP and MinIP as described in chapter 2.2.1. By taking the absolute difference between these, a difference image is created. This will then be a visualization of the maximum difference in attenuation during the scan, and is the image to be used in the segmentation.

To preserve the edges, but reduce noise, a bilateral filtering as described in [32] is performed as a preprocessing step. This is shown in Figure 19.

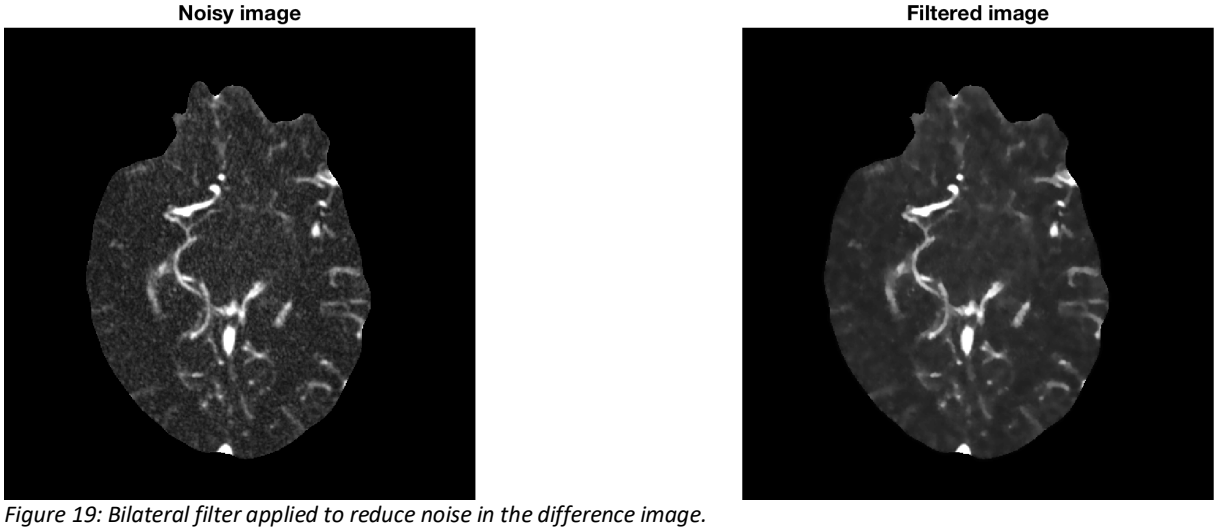

Figure 19: Bilateral filter applied to reduce noise in the difference image.

Another property that can be exploited is the shape of the vessels. A filter developed to enhance vessel-like structures is applied [33].

The segmentation of the vessels is performed on the difference images mentioned in 4.2.4.1. The idea is to find the vessels by using the information available in the time density curves. The vessels are assumed to be characterized as the pixels with the largest change in attenuation.

Input: All temporal images in a slice, *ImAll*

1. [MinIP,MIP] = minimum and maximum of ImAll in the t direction.
2. Imdiff = |MIP-MinIP|
3. B = Apply vessel enhancement filter to Imdiff
4. BW = Apply adaptive thresholding to B.

Output: Binary mask, BW

Algorithm 6: Finding vessel candidate segments with difference image and adaptive thresholding

4.2.4.3 Segmentation using feature extraction and clustering

Inspired by the work of Meijs et al. [25], a possible vessel segmentation method without ground truth available is to perform a clustering of the non-zero pixels, i.e. the tissue. The idea is that if proper features that describe vessels are used, the tissue can be divided into vessel and non-vessel pixels. As the largest amount of pixels will be non-vessels, the cluster containing least observations will correspond to the vessel cluster.

The features that are used are the temporal average and variance, the local entropy and standard deviation of the temporal variance and the first temporal image as described in [25]. Notice that the temporal average and variance images not are weighted as suggested in [25]. This is not necessary since all the temporal images for a patient have the same exposure in the given dataset. The features are visualized in Figure 20. In addition, the difference image

and the output of the vessel enhancement filter B [33] as described in chapter 4.2.4.2 are used.

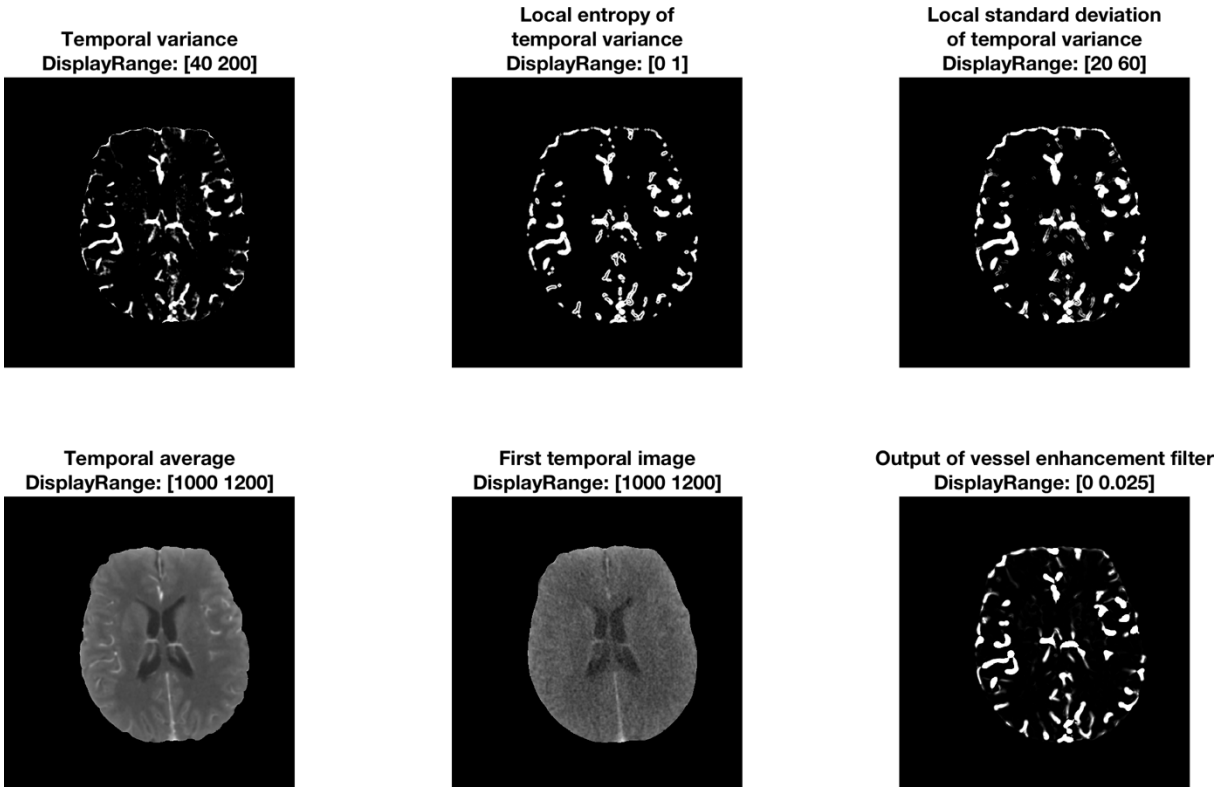

Figure 20: Different features that can be used in a clustering-based segmentation approach.

As these features seems to accentuate the regions where the vessels are located, these seem promising to use in the feature-based segmentation. Thus, the proposed method is described in Algorithm 7.

Input: *Imdiff*, *B*, *ImAll*

1. TV = The variance of ImAll in the temporal direction.
2. TA = The average of ImAll in the temporal direction.
3. TV_STD = Local standard deviation of the TV.
4. TV_E = Local entropy of the TV.
5. Im1 = First temporal image.
6. D = Feature vector containing [Imdiff, B, TV, TA, TV_STD, TV_E, Im1].
7. C = Kmeans clustering of D.
8. BW = Binary mask containing the cluster with least elements.

Output: Binary mask, *BW*.

Algorithm 7: Finding vessel candidate segments with clustering of features that accentuate vessel-like regions.

4.2.4.4 Remove segments

Since the time-density curve of a vessel is expected to be shaped as a bell, it is useful to do a curve fitting of the data points. Assuming uniform sampling, the TDC can be described by a Gaussian function on the form

$$y(x) = ae^{-0.5\left(\frac{x-b}{c}\right)^2} + d,$$

where a is the maximal change or the peak in attenuation, b is the time to peak, c is the standard deviation and d is an offset along the y-axis. Since uniform sampling is assumed in the fitting, the sample number is used on the time-axis. Figure 21 shows a curve fitting applied to a time-density curve derived from a vessel segment.

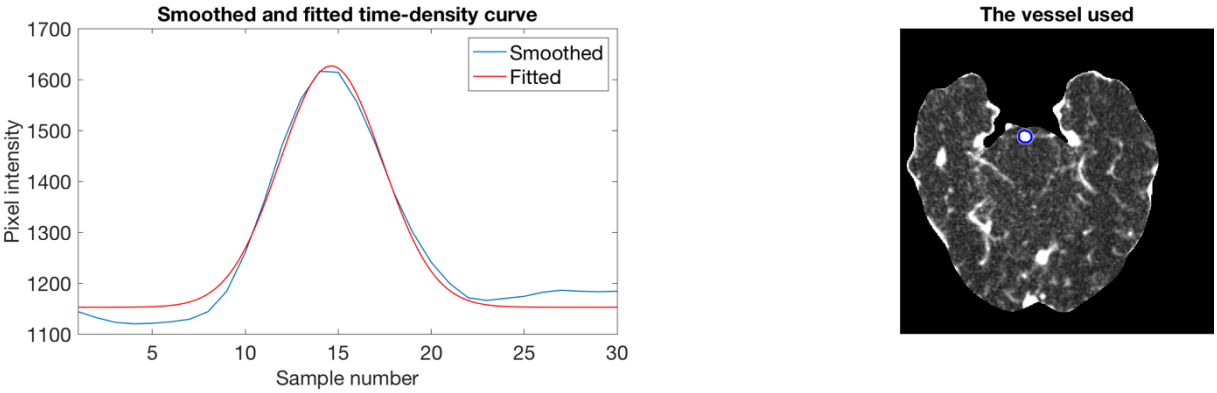

Figure 21: Example of curve fitting of a TDC of a given vessel.

The parameters obtained from the fit can be used as exclusion criteria and error checking for the segments. Example of a bad fit is shown in Figure 22. If any of the are outside the range of what is reasonable, the segment is probably not a vessel. Another property that can be obtained from the curve fitting, is the goodness of fit. Thus, a segment is excluded if any of the following conditions are satisfied:

- R-square less than 0.85
- Offset (d) greater than 1250 or less than 900
- Attenuation (a) less than 15
- Time to peak (b) less than 6 or greater than 29
- Absolute value of standard deviation (c) larger than 7.5

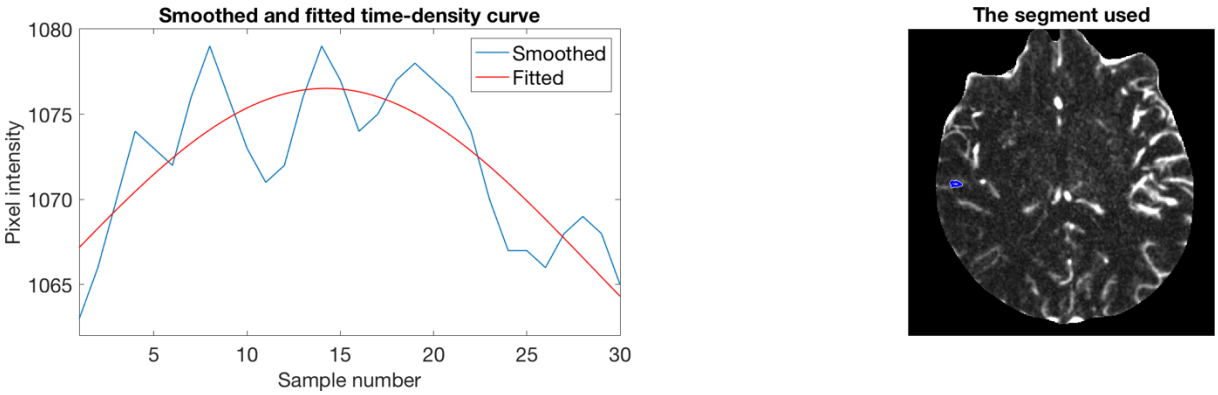

Figure 22: Example of an excluded segment. Since the time-density curve fits bad to a Gaussian, it is likely not a vessel.

4.2.4.5 Clustering to differentiate vessels

When the segments containing the vessels are identified, the next step is to determine which category each vessel belongs to, i.e. if it is either an artery or a vein. The arteries will be the pixels that change first, and the veins will be the pixels that change last. In addition, the change in attenuation will help distinguish between the types, as the arteries will have a smaller increase than the veins.

Since the dataset comes unlabeled, i.e. there is no ground truth available, training and evaluating a classification system is not possible. Instead, it is possible to do a clustering that tries to cluster the data into different classes based on the underlying relations in the dataset.

To prepare the data for clustering, it is necessary to perform a standardization of the features. This is due to the difference in scale between them. Applying the z-score normalization defined in as

$$x_{new} = \frac{x - \mu(x)}{\sigma(x)}$$

to each feature, where $\mu(x)$ and $\sigma(x)$ denote the measured mean and standard deviation, they are given equal expectancy $\mu = 0$ and standard deviation $\sigma = 1$.

To cluster the feature vectors, a k-means clustering is performed to cluster the features into two possible clusters. The squared Euclidean distance is the metric to minimize.

4.3 Implementation

All methods are implemented in MATLAB r2018a using mainly the *Image Processing Toolbox*, the *Statistics and Machine Learning* Toolbox and the *Wavelet Toolbox*. The toolbox *Fast mutual information of two images or signals* developed by J. Delpiano [34] is used to compute the mutual information in the registration. Five lines of code from [30] are used to improve the Watershed segmentation in the skull removal, and to divide vessel segments into smaller parts.

5 Experiments and results

5.1 Segment parametric maps

The first experiment is to validate if the method is able to determine which hemisphere the stroke lies in. The results are presented in Table 4.

Patient	01	02	03	04	05	06	07	08	09	10	11
Suggested	R	L	R	R	R	L	L	R	L	L	R
Truth	R	L	R	R	R	L	L	R	L	L	R

Table 4: The hemisphere where the stroke is located for each patient. Hemisphere suggested by the method, and truth.

As there are no errors, the method is able to detect which hemisphere the stroke is located in for all of the patients.

To evaluate the method's ability to estimate the amount of tissue at risk, the total area of the penumbra estimated is compared to the expert's opinion. This is shown in Figure 23.

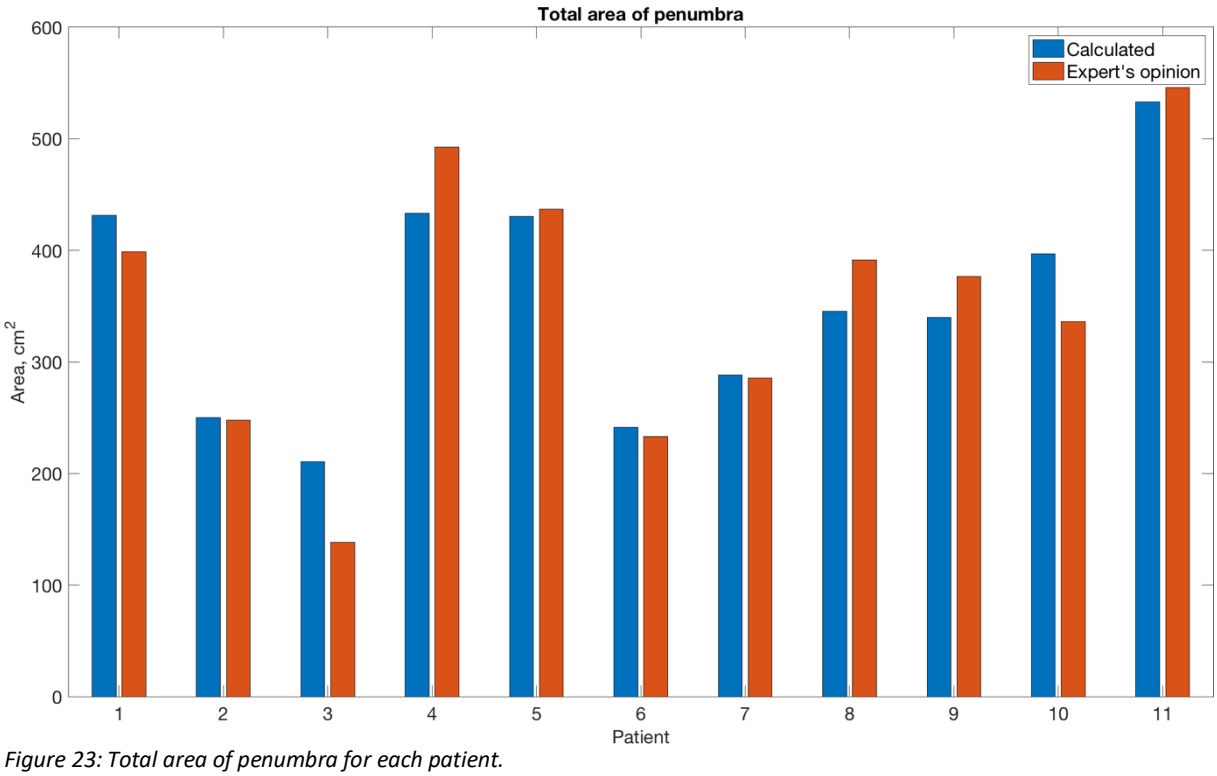

Figure 23: Total area of penumbra for each patient.

By visually interpreting the result, the estimated area is greater than the expert's opinion for four of the patients. The estimate is less than the expert's opinion for five of the patients. However, there is not much difference. For two of the patients, the calculated area and the expert's opinion are pretty similar. Based on this result, the method seems to give a decent estimate of the total area of the tissue at risk.

To evaluate the method's ability to estimate the amount of irreversibly damaged tissue, the total area of the estimated infarct core is compared to the expert's opinion. rCBF<30% of the blood flow in the healthy hemisphere is set as the threshold for the infarct core. The results are shown in Figure 24.

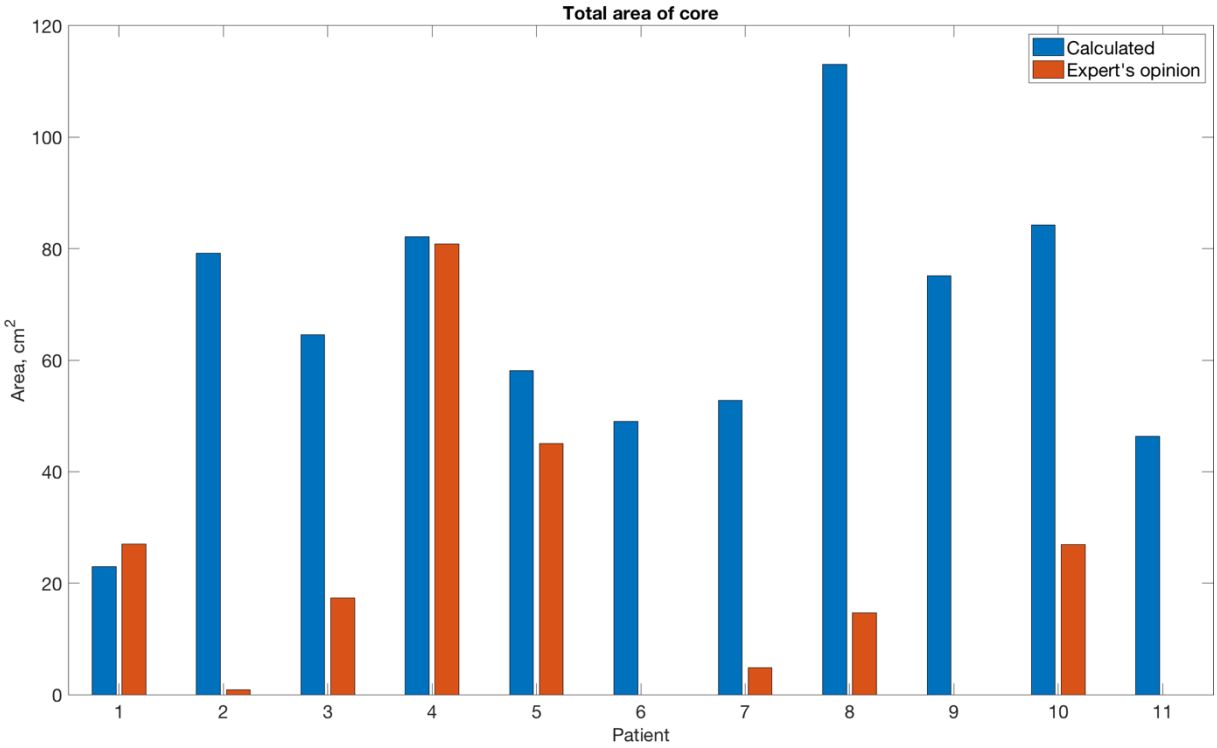

Figure 24: Estimated infarct core area when using rRBCF<30% as threshold, compared to the expert's opinion.

This is not as promising as the penumbra estimate. The method tends to overestimate the area of the infarct core for most of the patients compared to the expert's opinion. The differences are significant, but decent estimates can be seen for patient 01 and 04.

If the threshold is set to rCBF<25%, this gives the results presented in Figure 25.

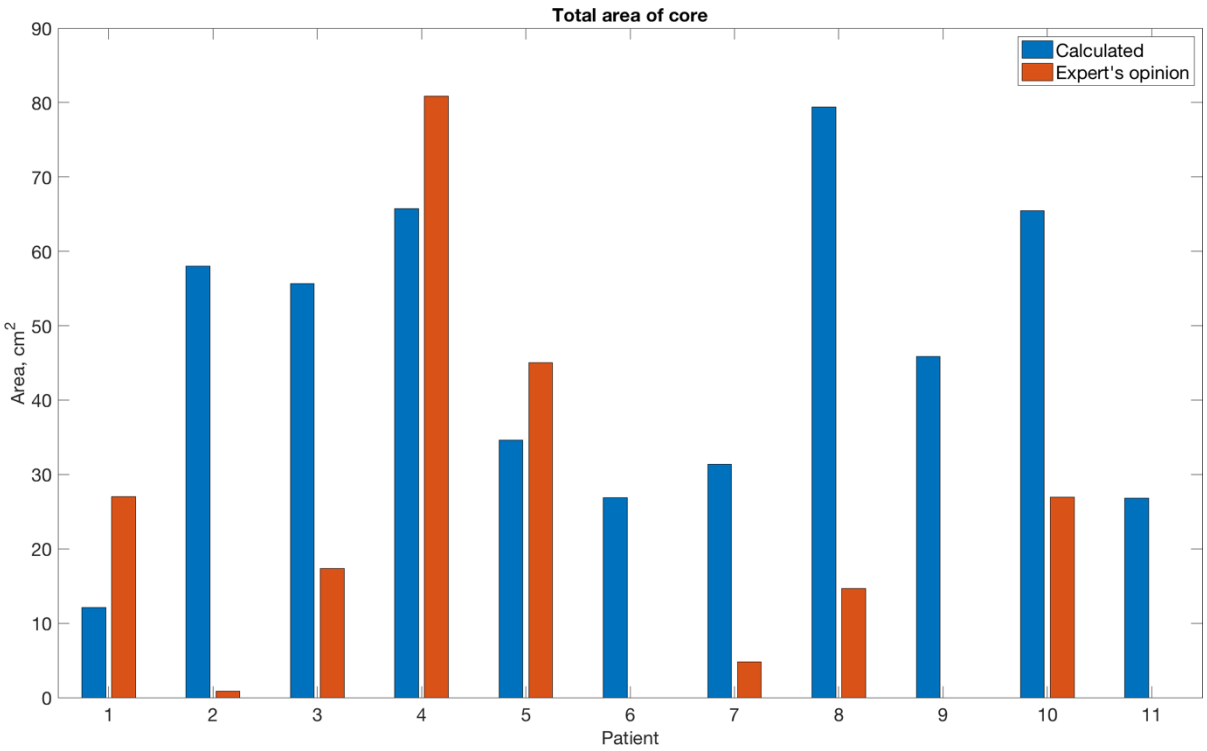

Figure 25: Estimated infarct core area when using rRBC<25% as threshold, compared to the expert's opinion.

The overestimation is reduced, but the method still gives poor performance. It might be better to use another parameter in the method to define the infarct core, and look at how this affects the estimated area. If CBV<1.25 is used, this gives the result presented in Figure 26.

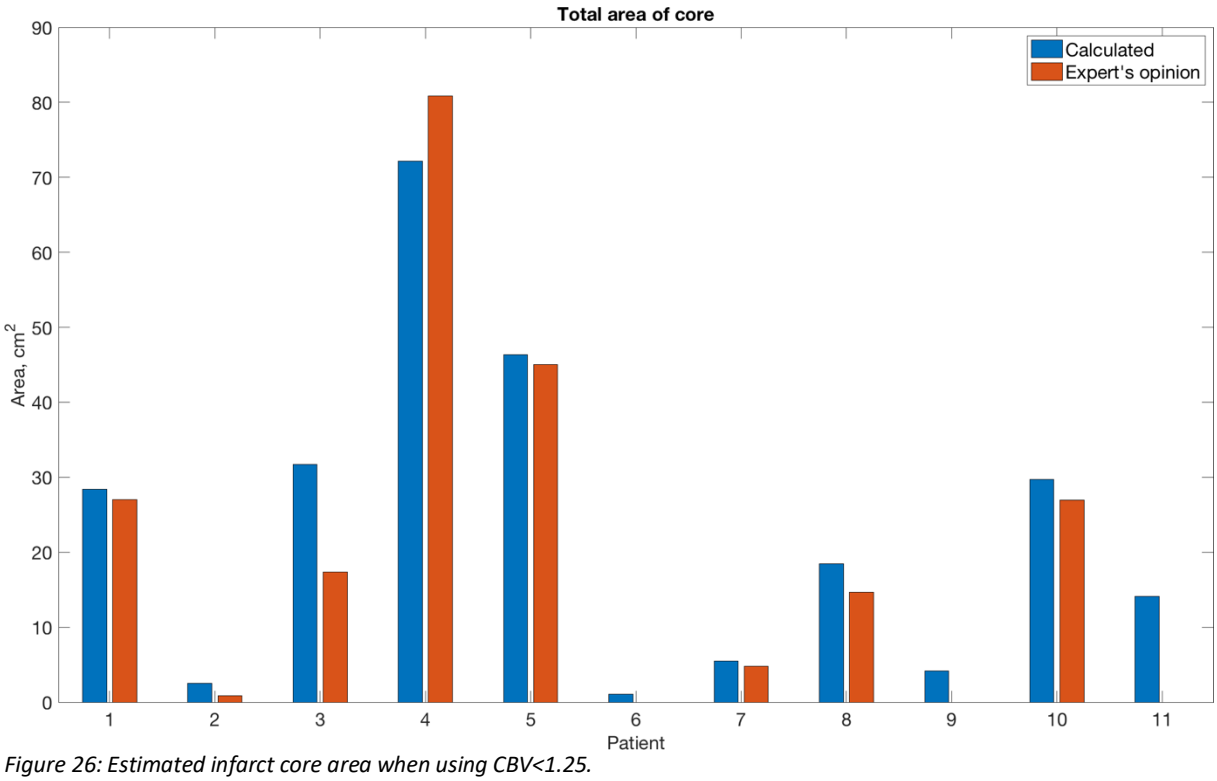

Figure 26: Estimated infarct core area when using CBV<1.25.

The estimated area and the expert's opinion is now less different for all of the patients. The overestimation is significantly reduced compared to when rCBF is used.

5.2 Registration of CT images

To determine which optimization algorithm and similarity metric to choose for further evaluation, two registrations are performed that treat the images as monomodal and multimodal images, respectively. The monomodal registration uses Regular Step Gradient Descent algorithm with the optimizer parameters in Table 5, and optimizes the Mean Squared Difference.

GradientMagnitudeTolerance	1.00e-04
MinimumStepLength	1.00e-05
MaximumStepLength	6.25e-2
MaximumIterations	100
RelaxationFactor	0.5

Table 5: Parameters when treating the images as monomodal images, with the Regular Step Gradient Descent Optimizer optimizing the mean squared difference. The default parameters in the Image Processing Toolbox are used as a starting point.

The multimodal registration uses the One-Plus-One Evolutionary algorithm, and optimizes the mutual information. The optimizer parameters used are found in Table 6.

GrowthFactor	1.05
Epsilon	1.5e-6
InitialRadius	6.25e-3
MaximumIterations	100

Table 6: Parameters when treating the images as multimodal images, with the One-Plus-One Evolutionary Optimizer optimizing the mutual information. The default parameters in the Image Processing Toolbox are used as a starting point.

As the optimizers are different, the only mutual parameter is the MaxiumItereations. All the parameters presented are the default parameters suggested in. This yields the result in Figure 27.

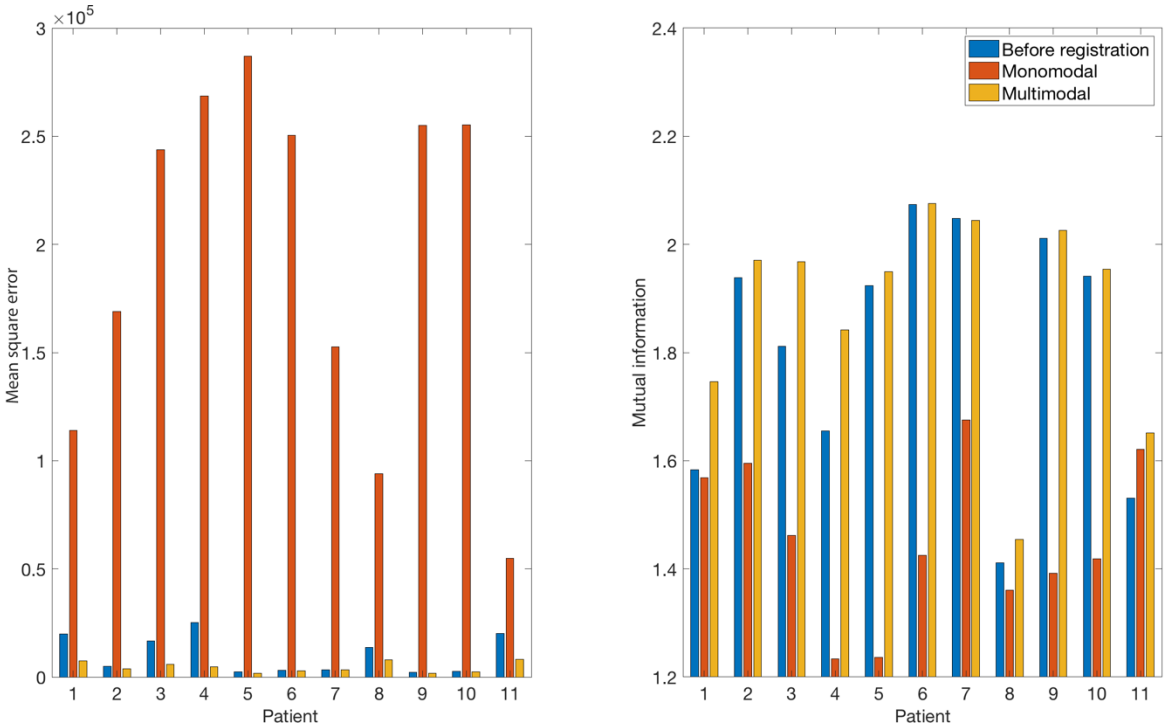

Figure 27: Similarity metrics when treating the images as monomodal and multimodal images with different optimizers.

The result clearly shows that treating the images as monomodal gives poor performance. In contradiction to the purpose of the registration, the mean squared error is actually increased compared to what it was before. In addition, the mutual information after is reduced compared to their values prior to the registration for all patients except number 11. From these results, the monomodal registration degrades the similarity between the images. Thus, this method is discarded, and the images will have to be treated as multimodal images, even though they come from the same scanner and modality. This is probably due to the change in contrast during the scan. The registration method selected for further evaluation is therefore the One-Plus-One evolutionary optimizer with the mutual information as the similarity metric to optimize. Notice that even though the mean squared error is not used as the metric to optimize, it is still significantly reduced.

To further improve the registration with respect to the similarity metrics, the parameters are adjusted by increasing the scaling factor to 2. This yields the new optimizer parameters found in Table 7.

GrowthFactor	Epsilon	InitialRadius	MaximumIterations
1.025	7.5e-7	3.125e-3	200

Table 7: Parameters with scaling factor 2.

As seen in Figure 30, there is a reduction in the mean squared error for all of the patients when the scaling factor is set to 2. In addition, the skull seems to align better when inspecting the error seen in Figure 28. The mutual information is also increased, but the change here seems to be smaller than for the other similarity metrics.

To see if the registration can be improved again, the scaling factor is now set to 4. This yields the new optimizer parameters seen in Table 8.

GrowthFactor	Epsilon	InitialRadius	MaximumIterations
1.0125	3.75e-7	1.5625e-3	400

Table 8: Parameters with scaling factor 4.

As the results show in Figure 30, there is another reduction present in the mean squared error. In addition, the alignment of the skull seems to be better, when inspecting the error in Figure 28. This tells that registration is improved. However, the mutual information is hardly changed, as seen in Figure 29.

To see if there are more improvements to gain, the scaling factor is set to 8. This gives the optimizer parameters presented in Table 9.

GrowthFactor	Epsilon	InitialRadius	MaximumIterations
1.00625	1.875e-7	7.8125e-4	800

Table 9: Parameters with scaling factor 8.

As the results show in Figure 30, the reduction in the mean squared error is significantly smaller when going from scaling factor 4 to 8 than from 2 to 4. The same goes for the reduction of the error, as seen in Figure 28. Based on these metrics, the registration is improved, but not as much as before. Again, the mutual information is hardly changed, as seen in Figure 29. Judging from these results, the registration is about to converge. Thus, a further increase in the scaling factor will probably not result in any large improvements in the registration performance.

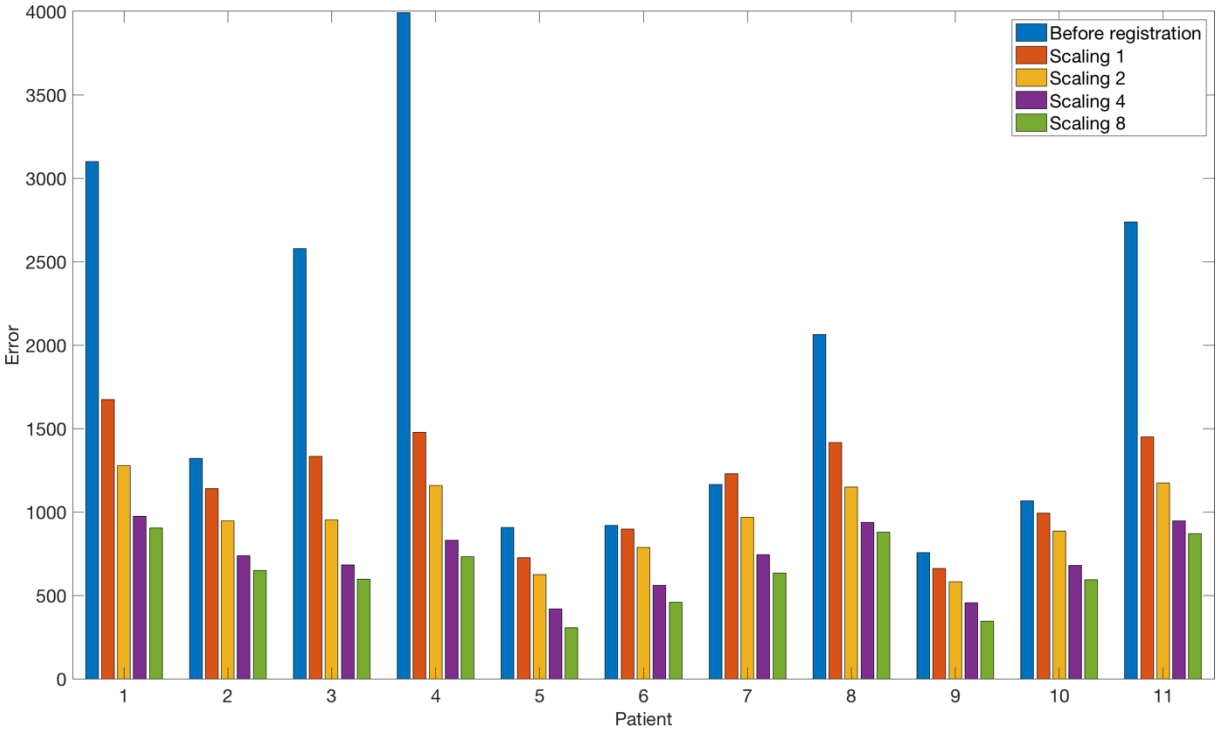

Figure 28: Error before and after registration.

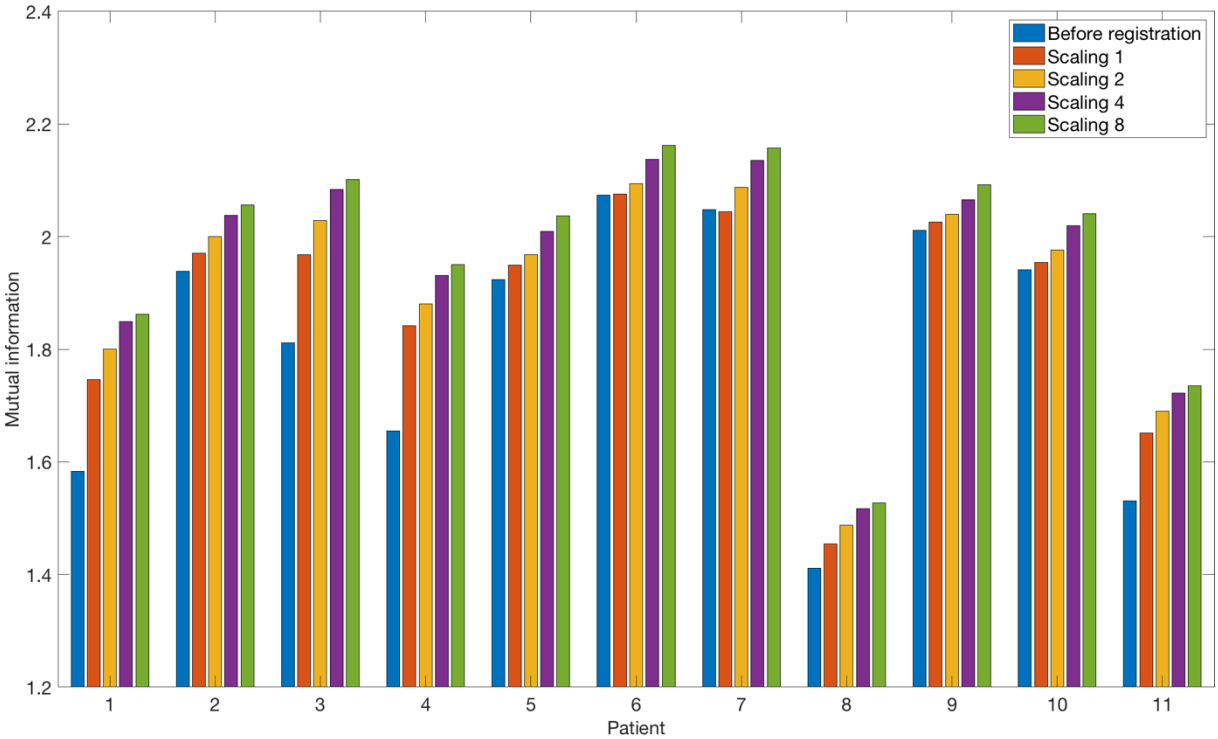

Figure 29: Mutual information before and after registration.

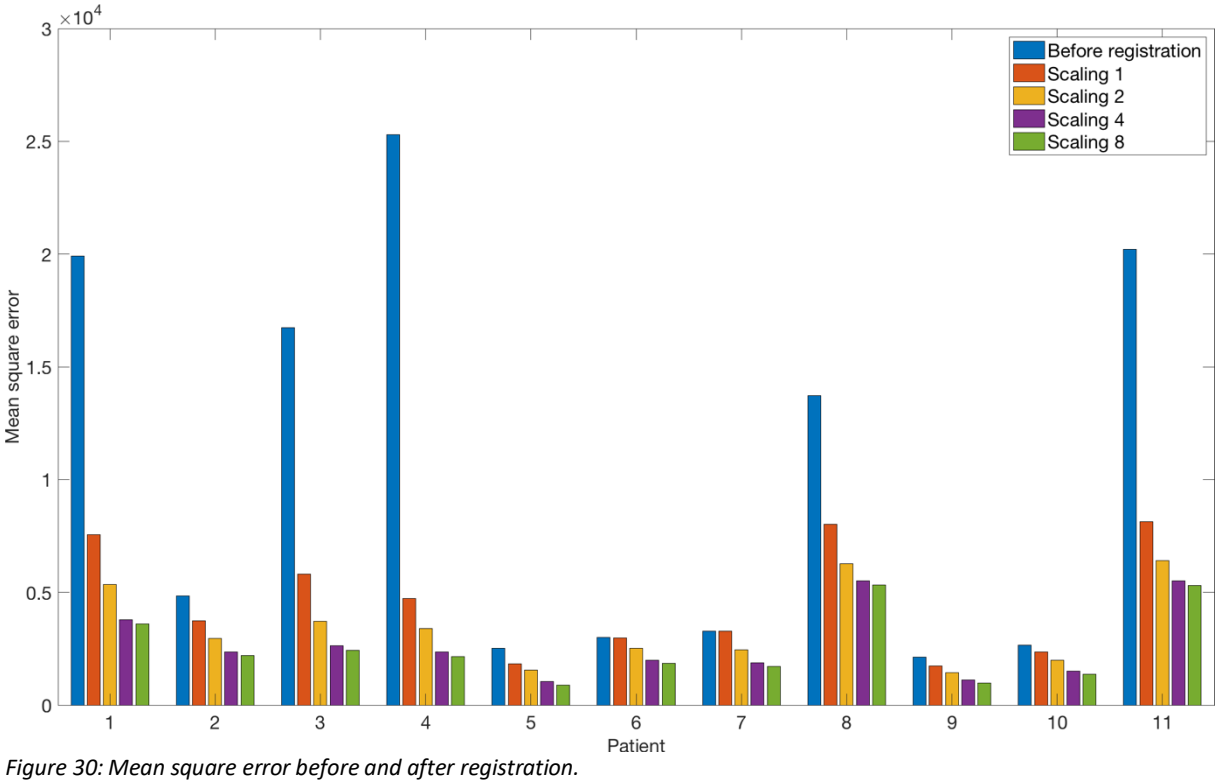

Figure 30: Mean square error before and after registration.

To get the best possible registration performance with this method, it would be better to tune and evaluate the influence of each of the parameters individually. The reason for not doing this, is that it is time consuming to do, as the optimization algorithm is iterative. Thus, it is not

particularly feasible to do with a limited amount of computational power. However, the method suggested with a single scaling factor has shown to be a simple way to improve the registration to some extinct.

The similarity metrics are useful to get a measure of the performance, but it is also useful to visually inspect the effect of the registration.

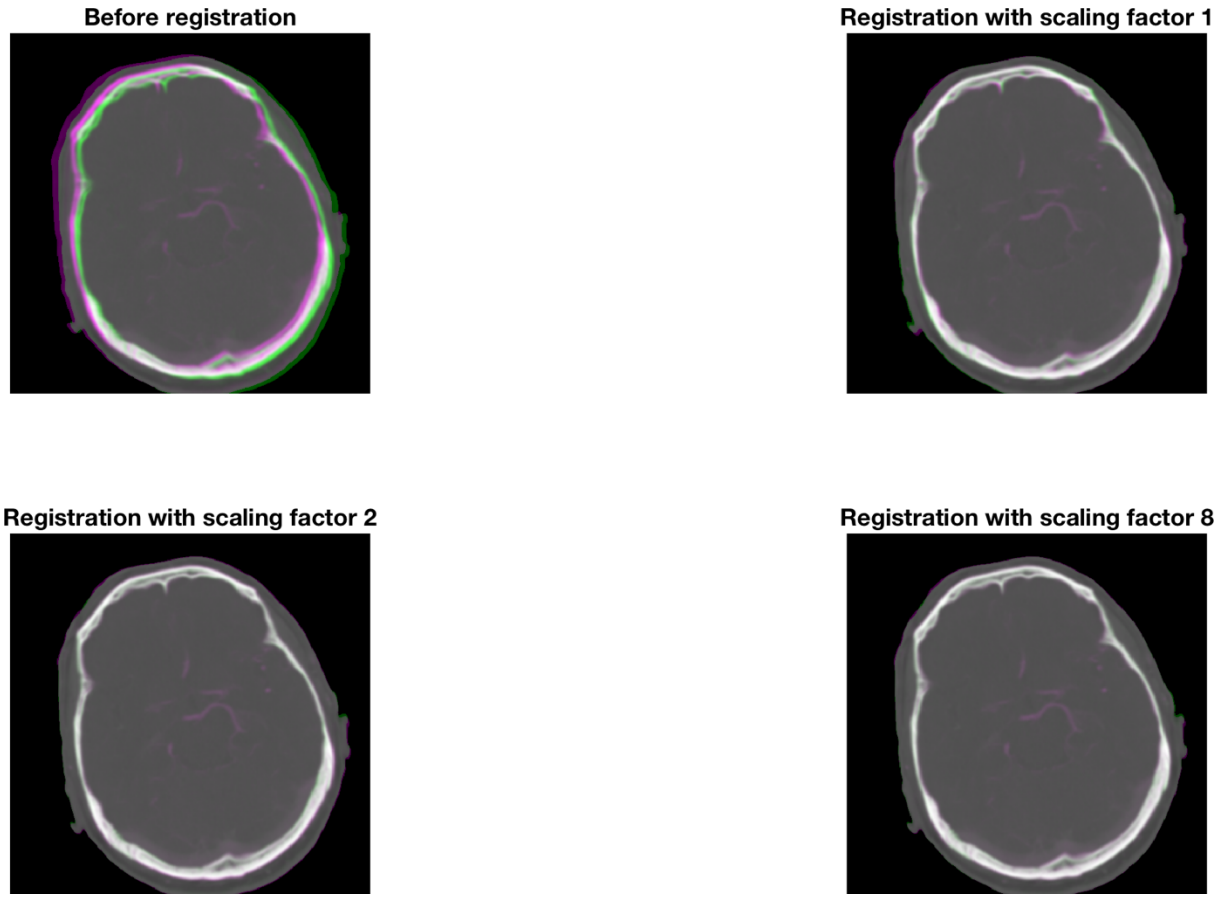

Figure 31: Images before registration and after registration with scaling factor 1, 2 and 8. Images from patient 4, slice 3. Differences between the images are colored as green and magenta.

By visual inspection, the registration clearly reduces the difference between the images. An interesting observation is the similarity between images registered with different scaling factors. It is hard to say which of the registrations performs best when inspecting comparing the registered images. There is also another important and interesting insight, which also can be seen from Figure 28, Figure 29 and Figure 30 containing the similarity metrics. The largest jump in similarity comes when the images are registered. The increase when tuning the parameters is way smaller.

5.3 Skull removal

5.3.1 Selection of wavelet

To select which wavelet to be used in the edge detection, several different wavelets are evaluated. This is done by visually inspecting the result of the edge detection, and then select the one which best accentuates the skull. 1 decomposition level is used as a starting point.

When choosing the Haar wavelet, this gives the detail coefficients seen in Figure 32

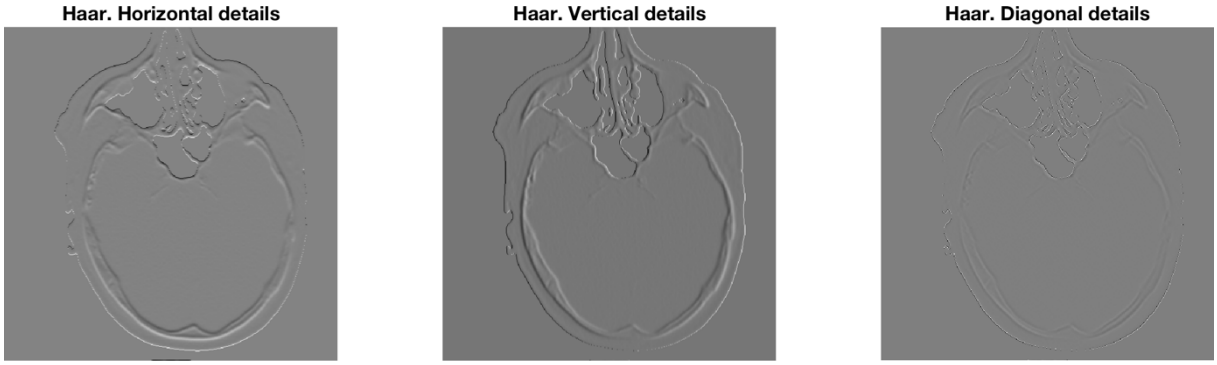

Figure 32: Detail coefficients when using the Haar wavelet.

The contours of the skull are clearly visible in both the horizontal and vertical details. There are also some diagonal details present. This implies that the Haar wavelet is suitable for detecting edges in the given images.

When choosing the Biorthogonal 2.2 wavelet, this gives the wavelet detail coefficients seen in Figure 33.

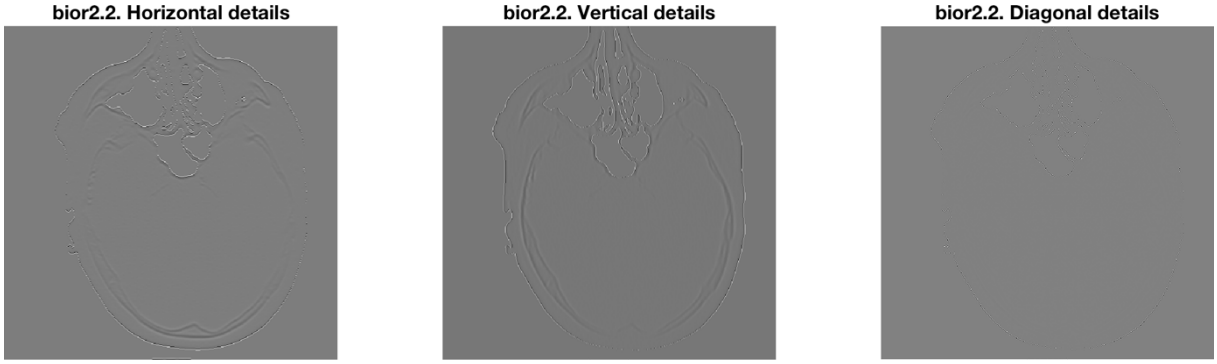

Figure 33: Detail coefficients when using the Biorthogonal 2.2 wavelet.

The contours of the skull are now less visible in all of the detail coefficients. Thus, this wavelet does not perform better than the Haar wavelet and is therefore not suited for detecting edges in the given application.

When choosing the Daubechies 2 wavelet, this gives the wavelet detail coefficients seen in Figure 34

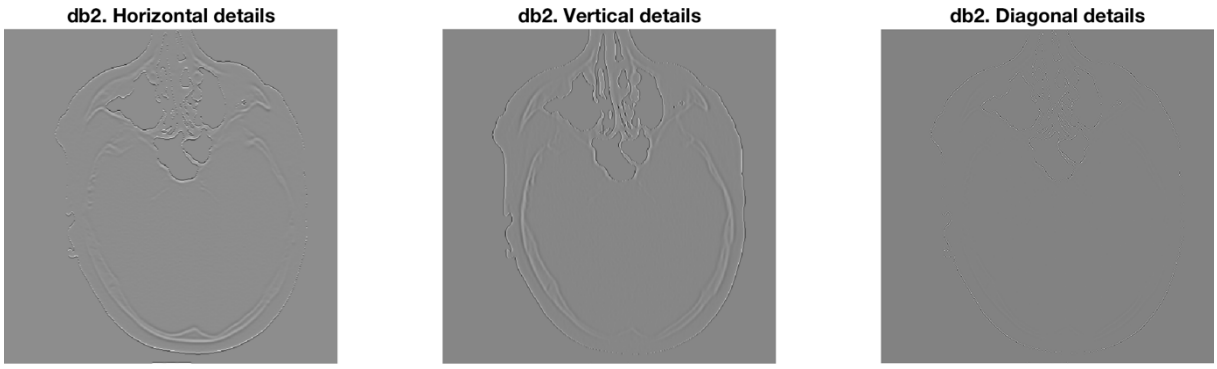

Figure 34: Detail coefficients when using the Daubechies 2 wavelet.

From this result, the Daubechies 2 wavelet performs slightly better than the Biorthogonal 2.2 wavelet. However, the performance is still worse than the Haar wavelet.

When trying the Discrete Meyer wavelet, this gives the wavelet detail coefficients seen in Figure 35.

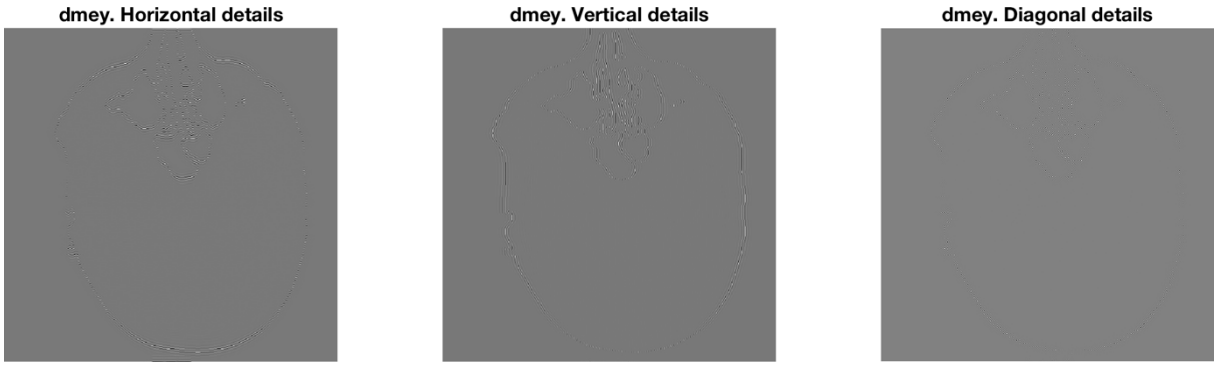

Figure 35: Detail coefficients when using the Discrete Meyer wavelet.

This result clearly demonstrates that the Discrete Meyer wavelet is not suitable for edge detection in the given application, as it hardly detects edges in any of the directions.

When choosing the Biorthogonal 1.5 wavelet, this yields the result presented in Figure 36.

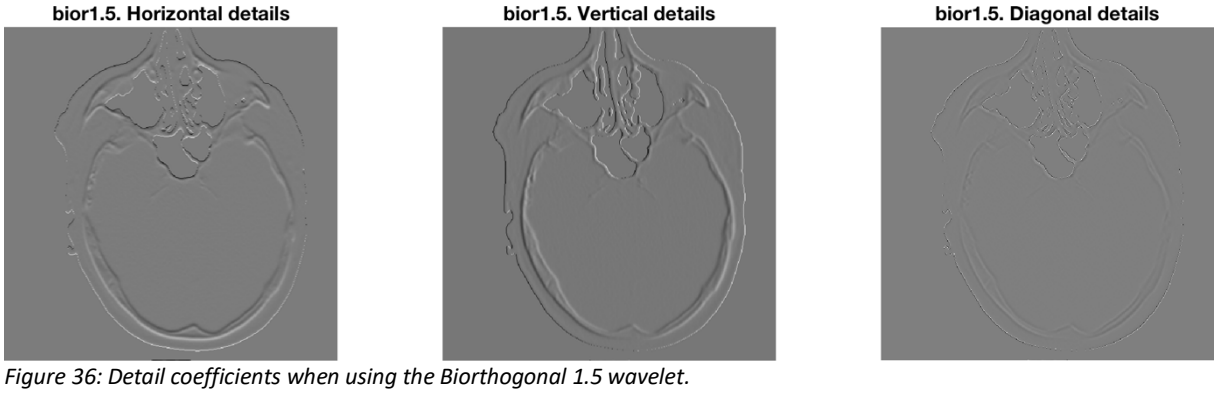

Figure 36: Detail coefficients when using the Biorthogonal 1.5 wavelet.

The performance of the Biorthogonal 1.5 is similar to the Haar wavelet. This is as expected, since the non-zero coefficients in the decomposition high-pass filters for the two wavelets are

equal. The only difference is the filter length. However, there is a difference in one of the slices as seen in Figure 37. The edge detected by the Biorthogonal 1.5 wavelet, seen as cyan in Figure 37, seems to correspond better to transition between the brain and the skull than the edge detected by the Haar wavelet, seen as red in Figure 37. Thus, the Biorthogonal 1.5 becomes the selected wavelet.

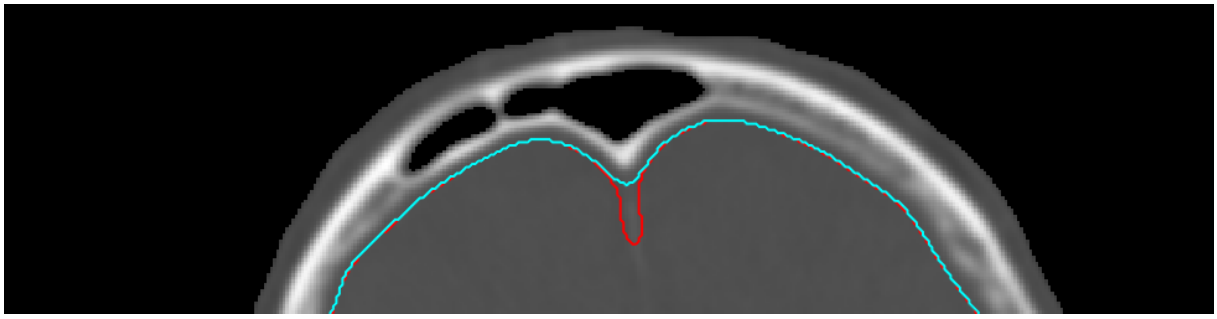

Figure 37: Cyan: Biorthogonal 1.5 wavelet used for edge detection. Red: Haar wavelet used for edge detection. Crop of patient 11, slice 14.

5.3.2 Result of the skull removal

To evaluate the performance of the skull removal, the resulting brain masks for the four lowest slices and then every other slice in patient 01 and 06 are presented. These are shown in Figure 38 and Figure 39, respectively. The result for the other patients are similar.

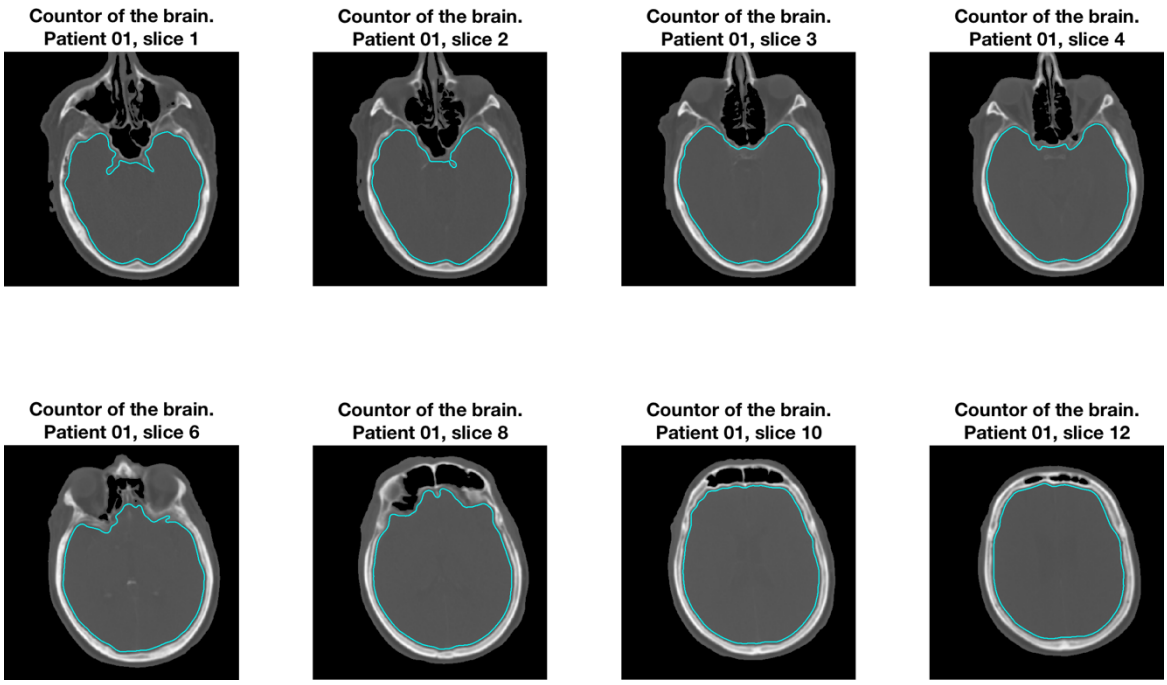

Figure 38: Contour of the brain found when patient 01's skull. The four lowest slices and then every other slice is presented.

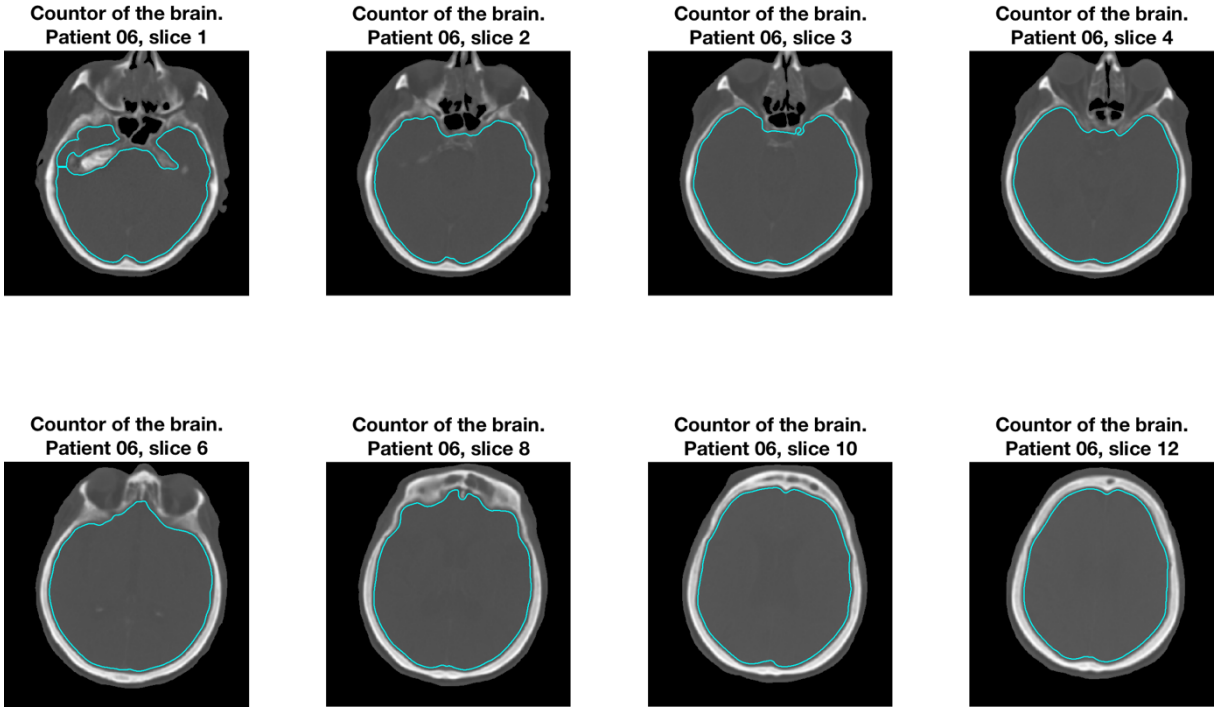

Figure 39: Contour of the brain found when patient 06' skull. The four lowest slices and then every other slice is presented.

5.4 Segment arteries and veins in CT images

The experiments will be to find the vessel candidate segments and thereafter remove the segments that likely not are vessels. With no ground truth available, the results of the vessel segmentation are best presented visually. Three slices from every other patient are presented. A slice where the vessels are particularly prominent is chosen for each patient in addition to the top and bottom slices.

5.4.1 Finding vessels in patient 01

The vessel segments found in slice 1, 5 and 13 for patient 01 are shown in Figure 40, Figure 41 and Figure 42, respectively.

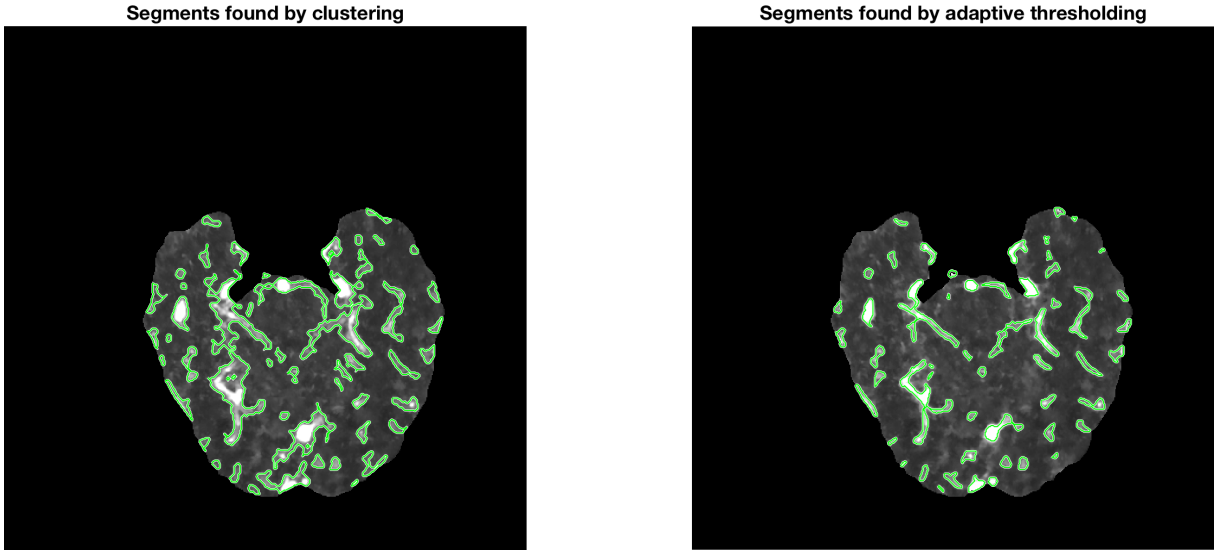

Figure 40. Vessel segments found in the bottom slice of patient 01.

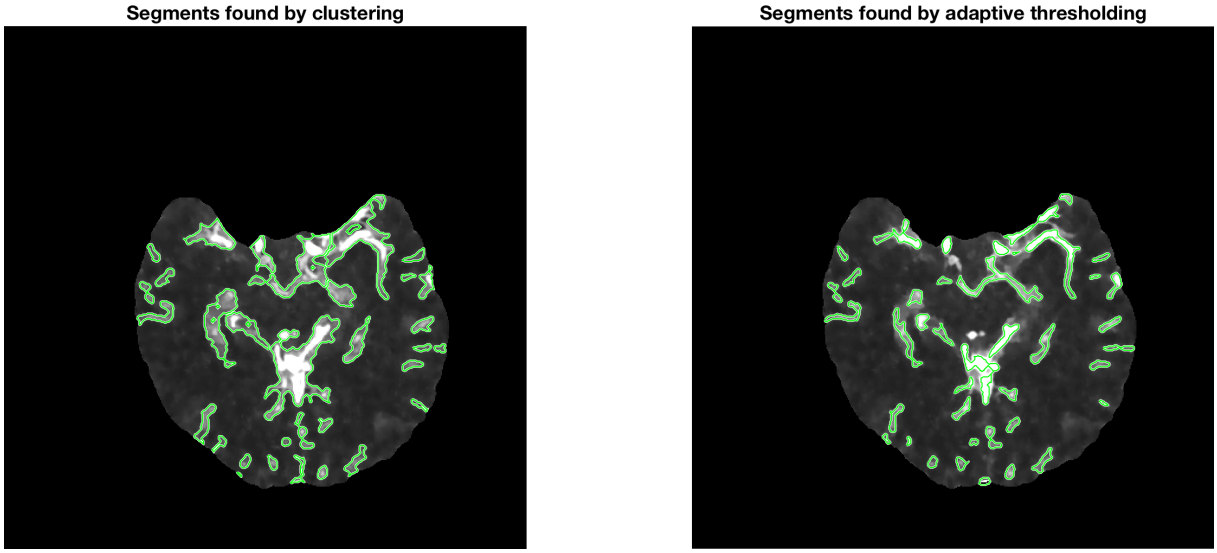

Figure 41: Vessel segments found in slice 5 of patient 01.

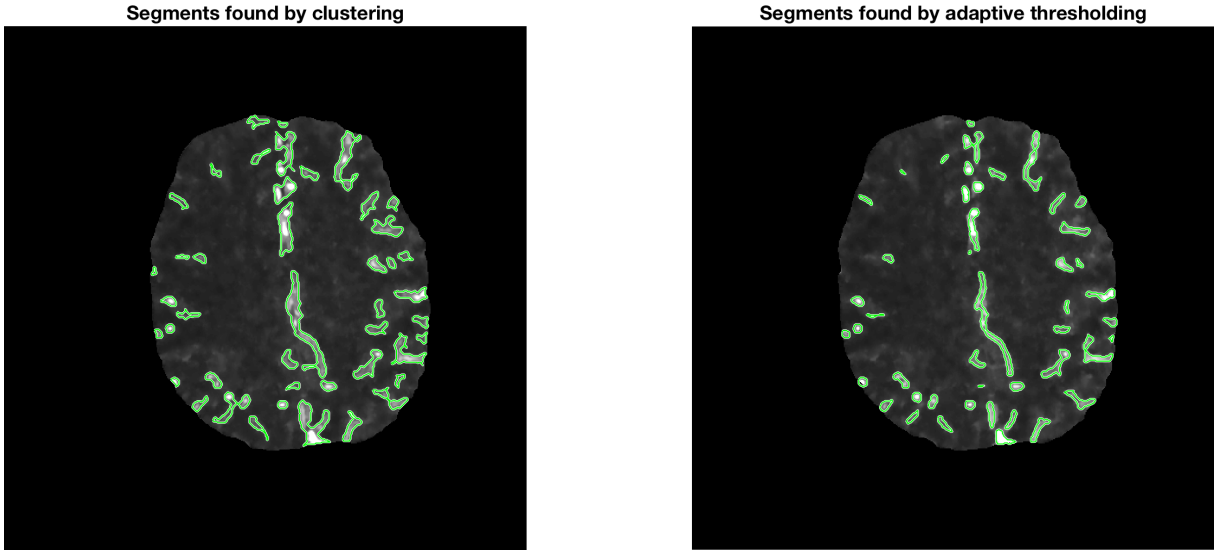

Figure 42: Vessel segments found in the top slice of patient 01.

5.4.2 Finding vessels in patient 03

The vessel segments found in slice 1, 5 and 13 for patient 03 are shown in Figure 43, Figure 44 and Figure 45, respectively.

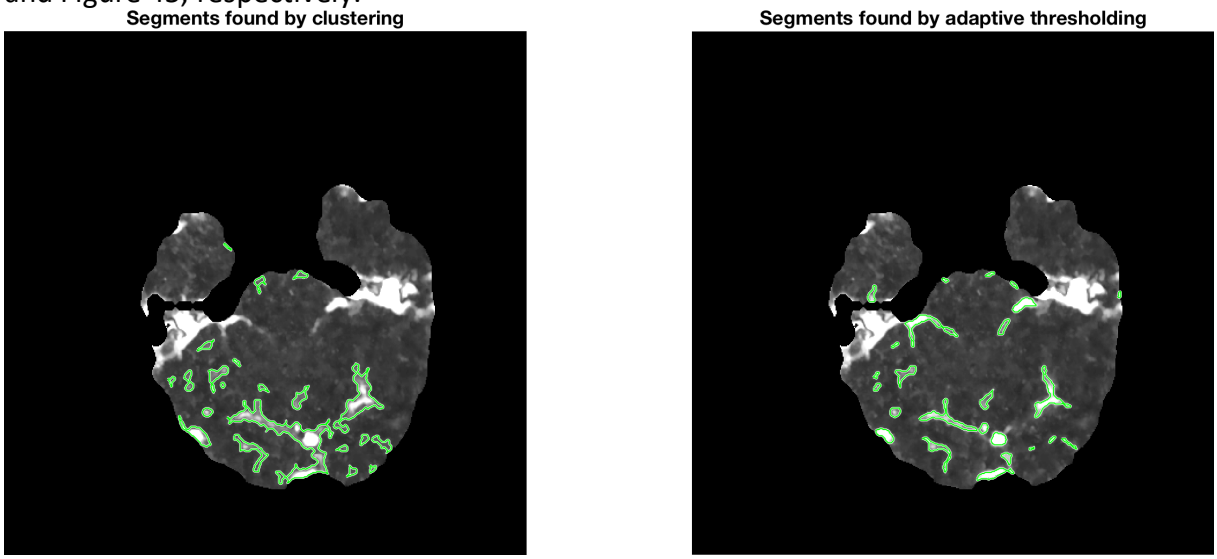

Figure 43: Vessel segments found in the bottom slice of patient 03.

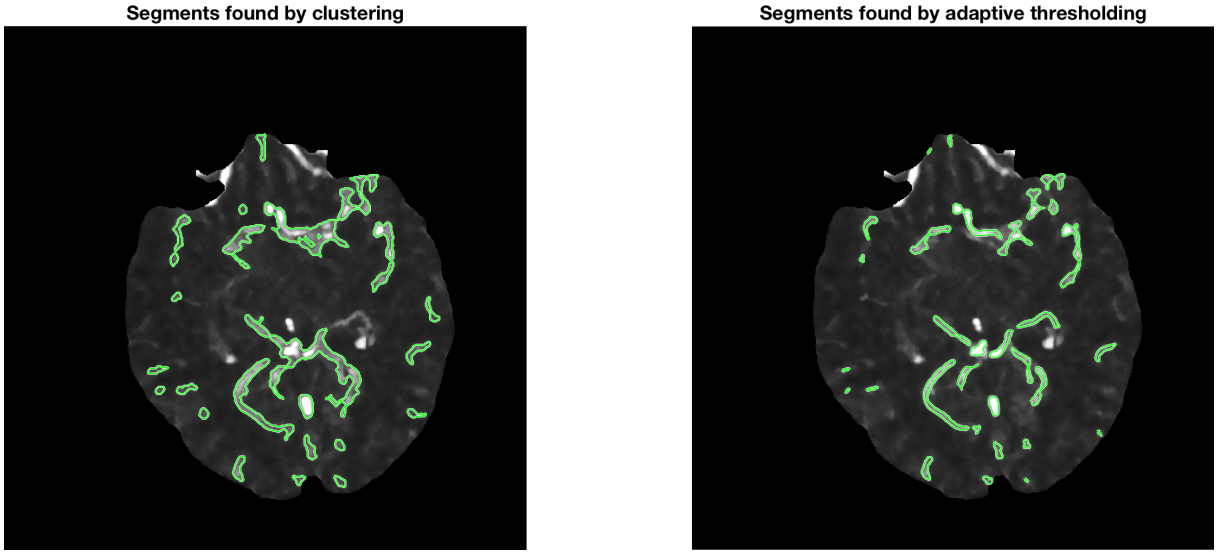

Figure 44: Vessel segments found in slice 5 of patient 03.

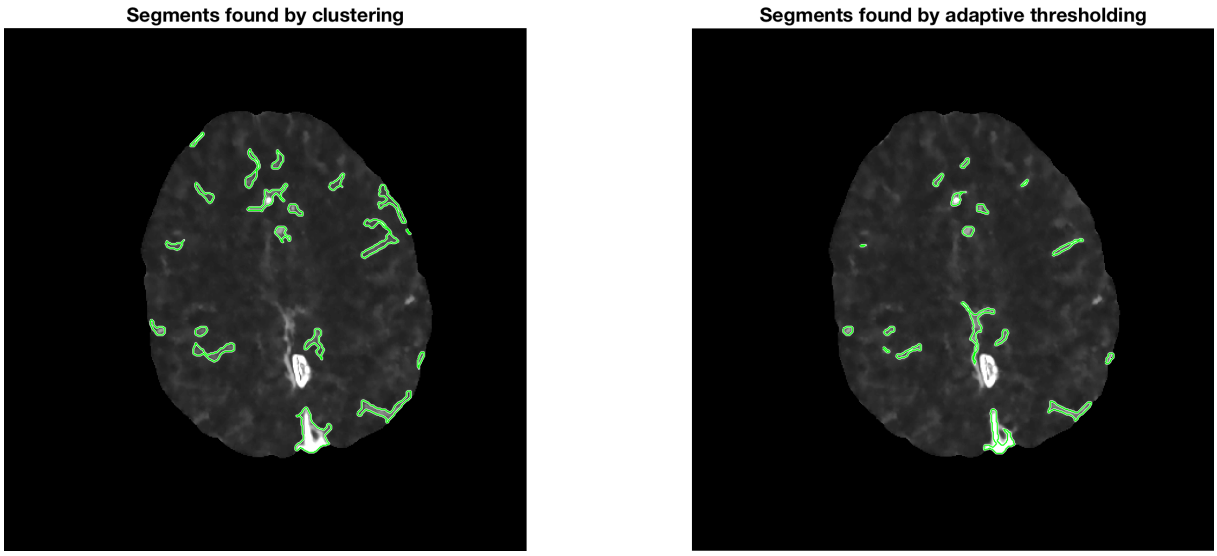

Figure 45: Vessel segments found in the top slice of patient 03.

5.4.3 Finding vessels in patient 05

The vessel segments found in slice 1, 4 and 13 for patient 05 are shown in Figure 46Figure 47Figure 48

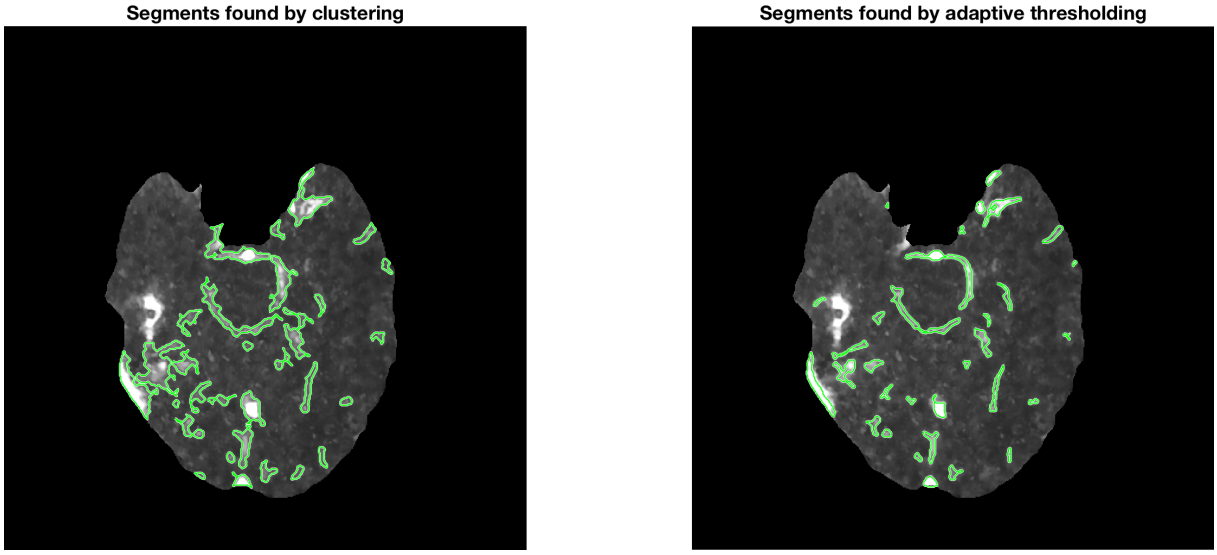

Figure 46: Vessel segments found in the bottom slice of patient 05.

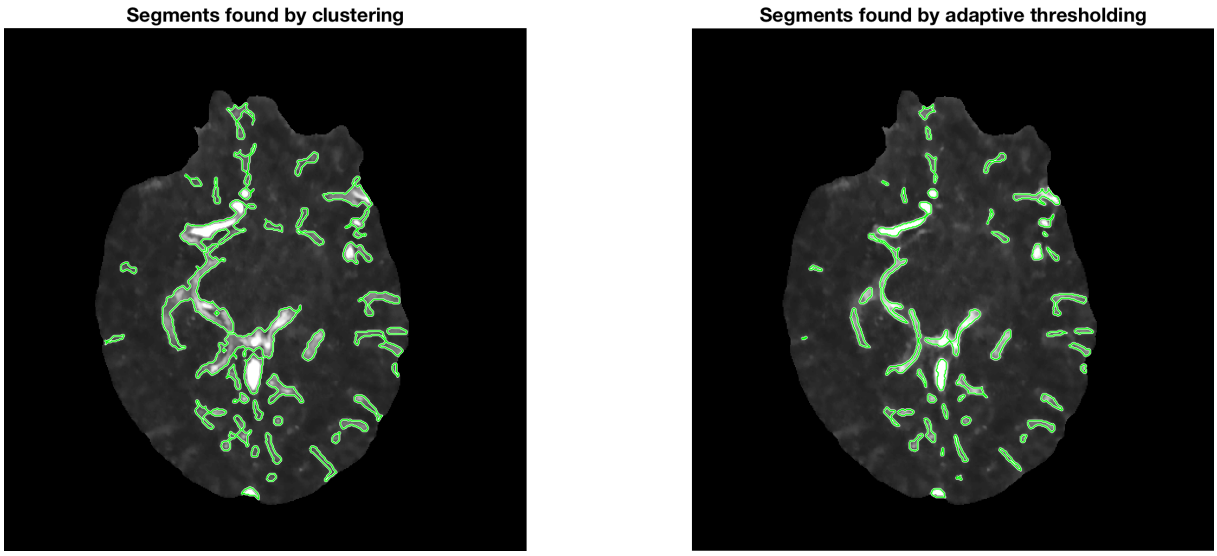

Figure 47: Vessel segments found in slice 4 of patient 05.

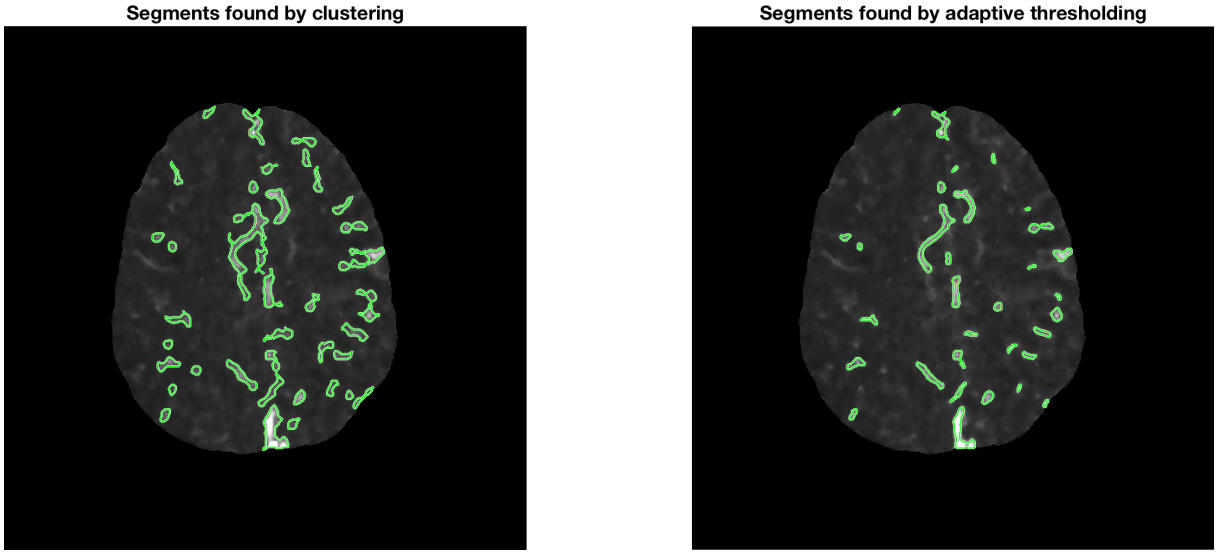

Figure 48: Vessel segments found in the top slice of patient 05.

5.4.4 Finding vessels in patient 07

The vessel segments found in slice 1, 5 and 13 for patient 07 are shown in Figure 49, Figure 50 and Figure 51, respectively.

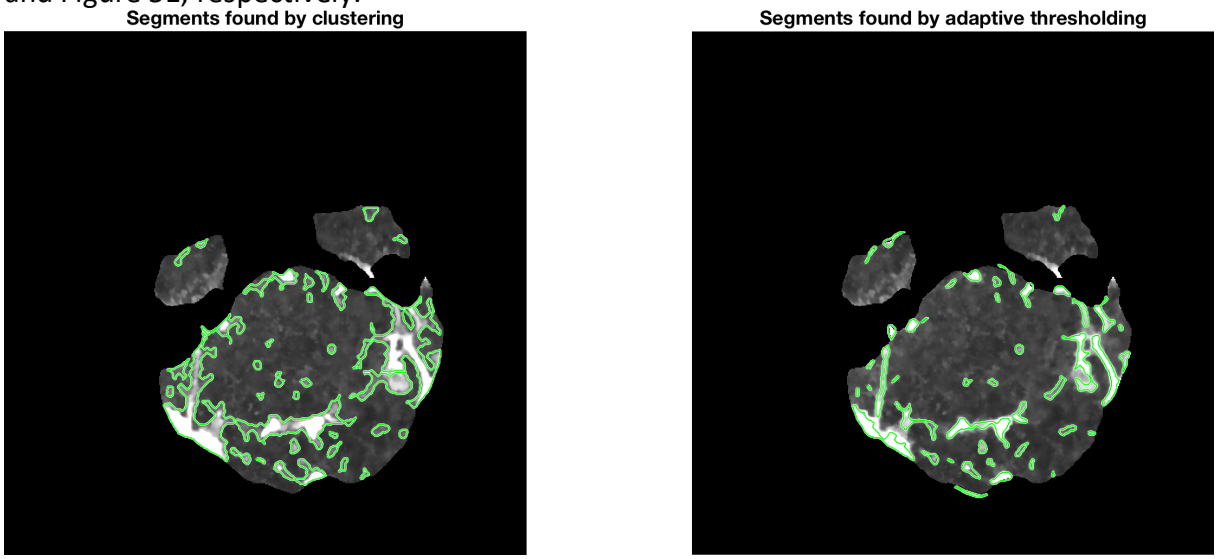

Figure 49 Vessel segments found in the bottom slice of patient 07.

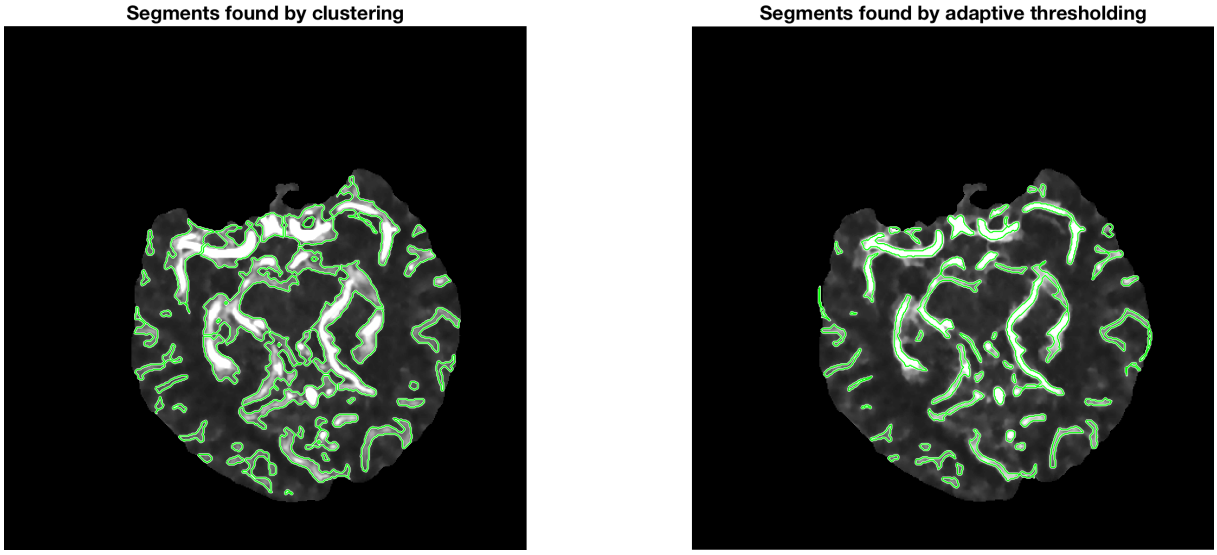

Figure 50: Vessel segments found in slice 5 of patient 07.

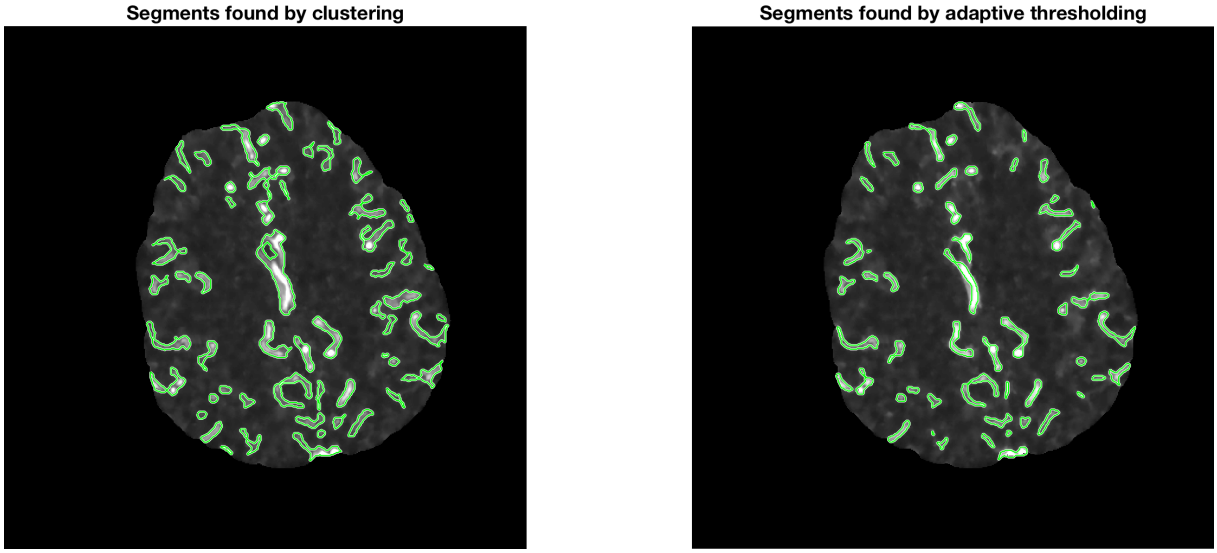

Figure 51: Vessel segments found in the top slice of patient 07.

5.4.5 Finding vessels in patient 09

The vessel segments found in slice 1, 3 and 22 for patient 09 are shown in Figure 52, Figure 53 and Figure 54, respectively.

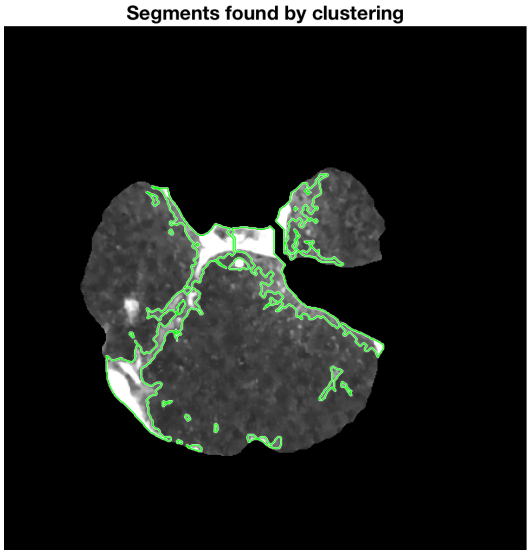

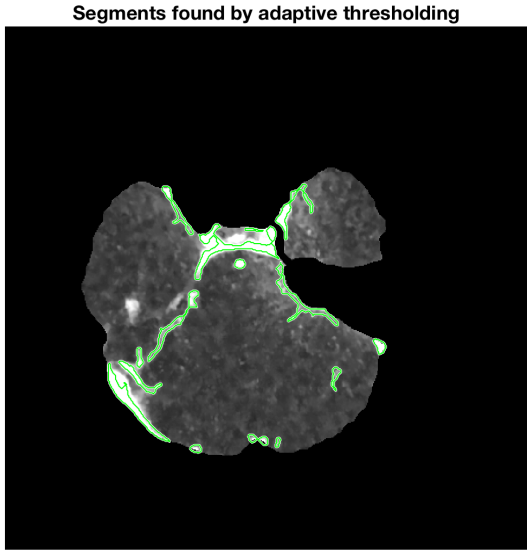

Figure 52: Vessel segments found in the bottom slice of patient 09.

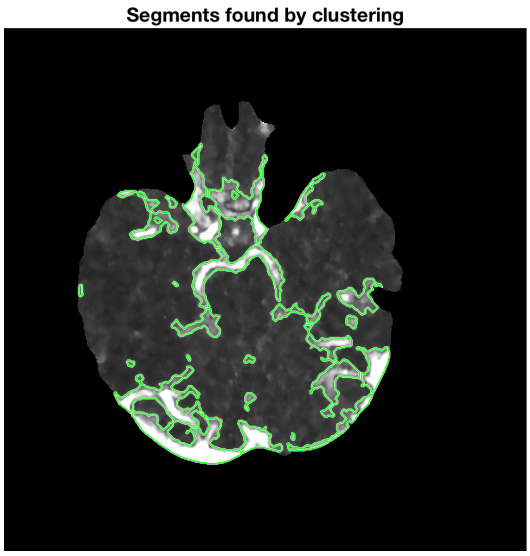

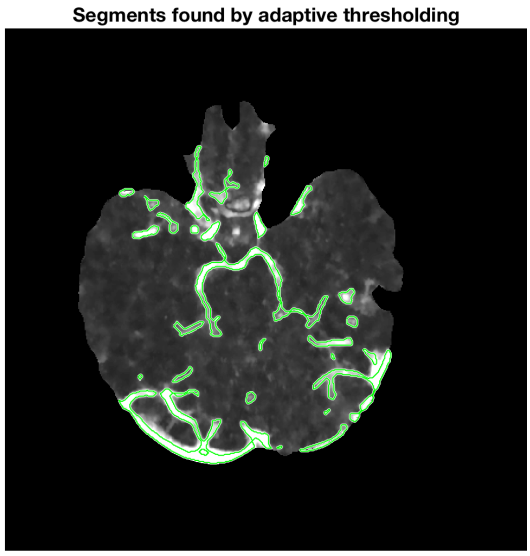

Figure 53 Vessel segments found the top slice of patient 11

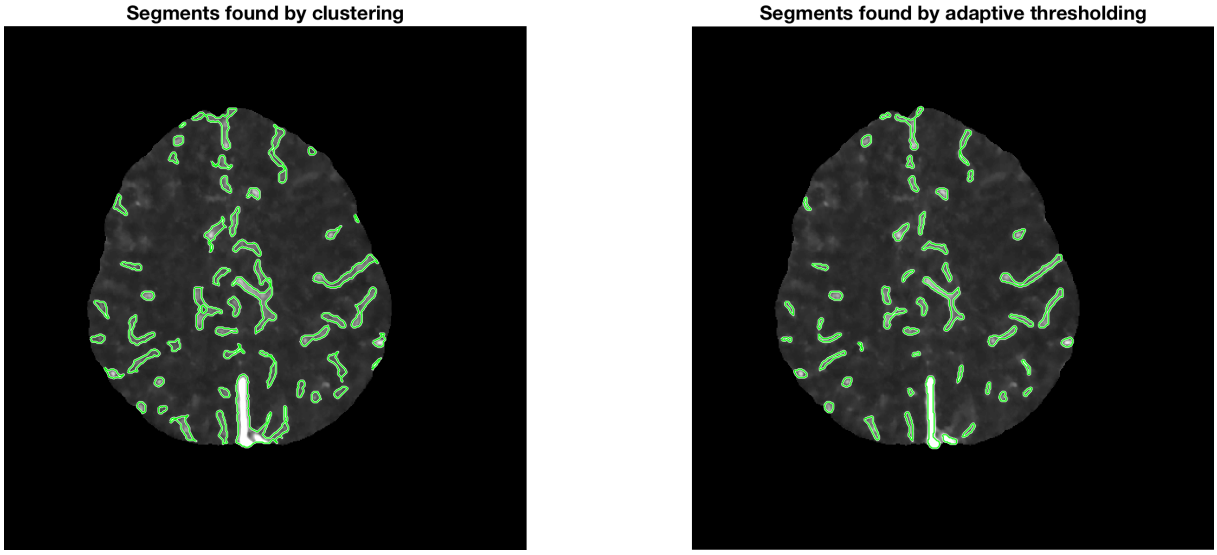

Figure 54: Vessel segments found in the top slice of patient 09.

5.4.6 Finding vessels in patient 11

The vessel segments found in slice 1, 5 and 14 for patient 11 are shown in Figure 55, Figure 56 and Figure 57, respectively.

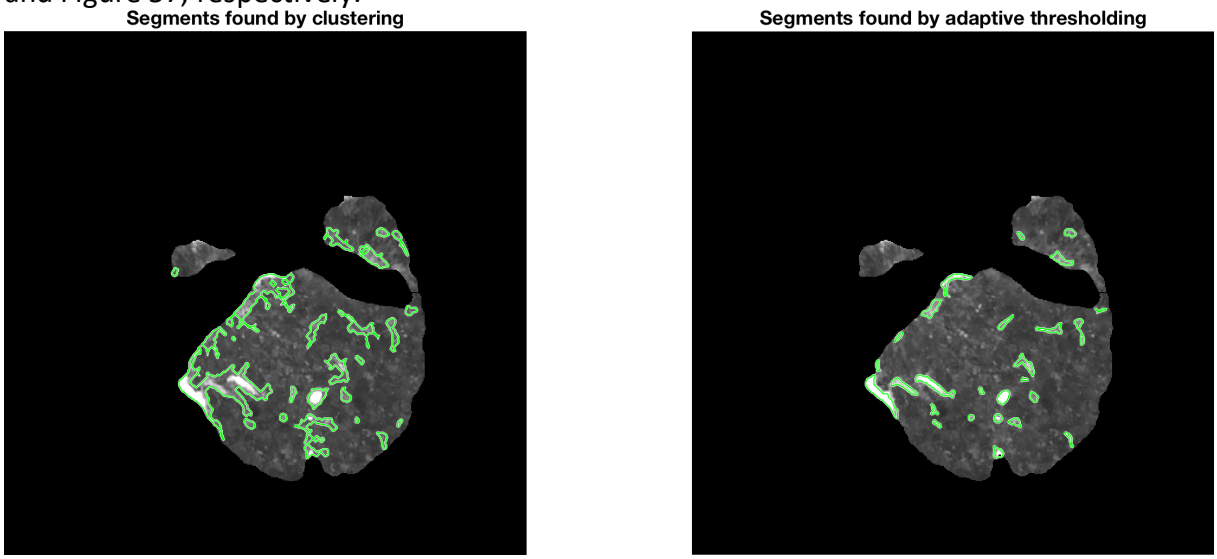

Figure 55: Vessel segments found in the bottom slice of patient 11.

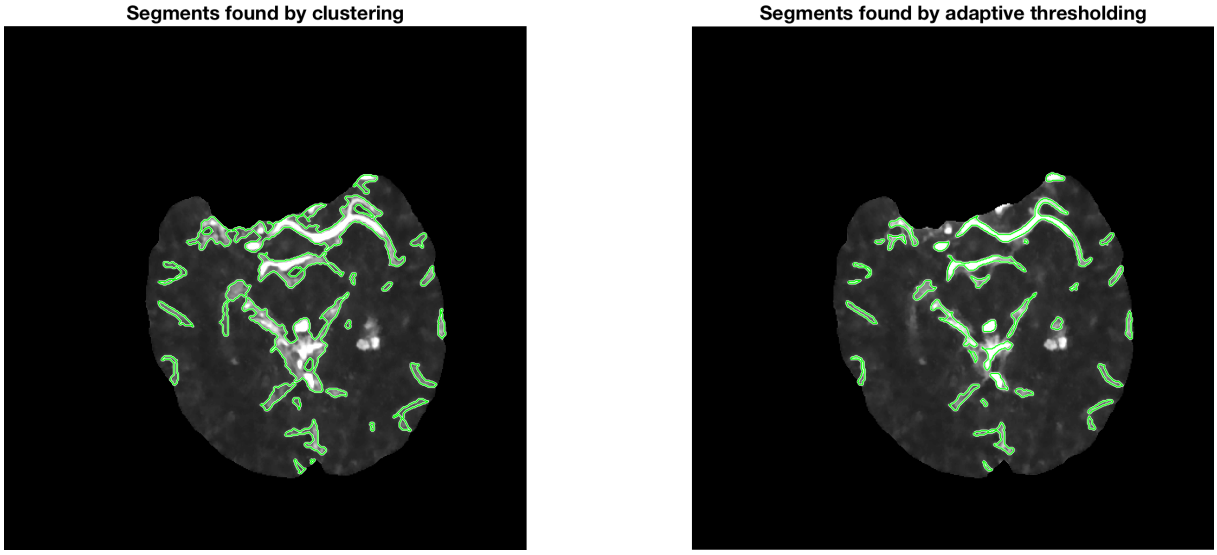

Figure 56: Vessel segments found in slice 5 of patient 11

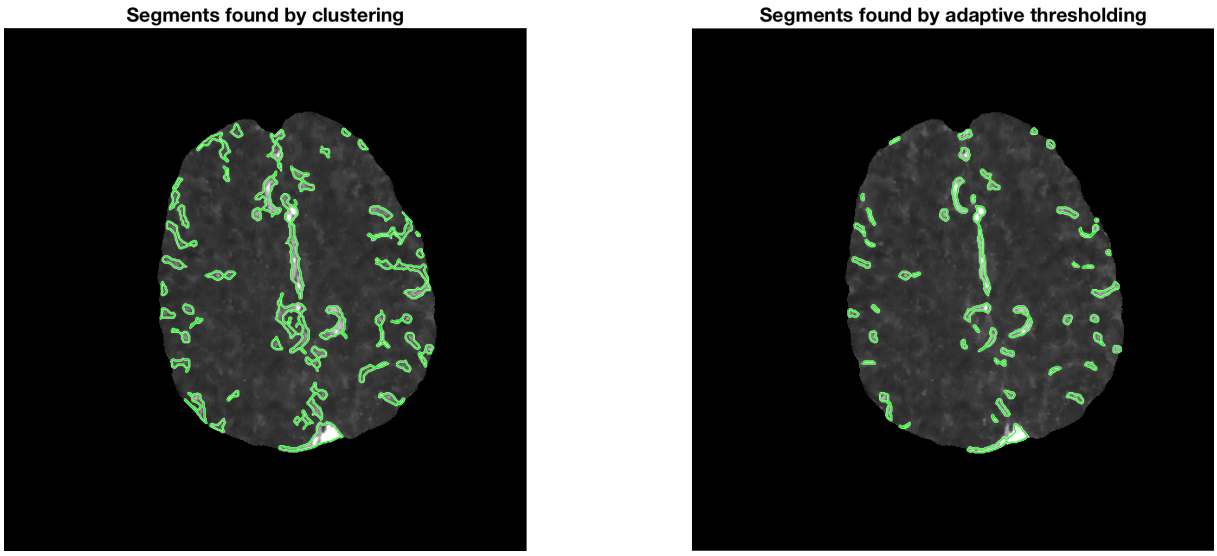

Figure 57: Vessel segments found in the top slice of patient 11.

5.4.7 Differentiating arterial and venous vessels

To differentiate the vessel segments, the following features are tested in a clustering:

(1) TTP and attenuation (A).

(2) TTP alone.

(3) Parameter b derived from the curve fitting and the attenuation (A).

(4) Parameter b alone.

Parameter b will then correspond to the time to peak when uniform sampling of the images is assumed. This results in the clusters for patient 01 presented in Figure 58.

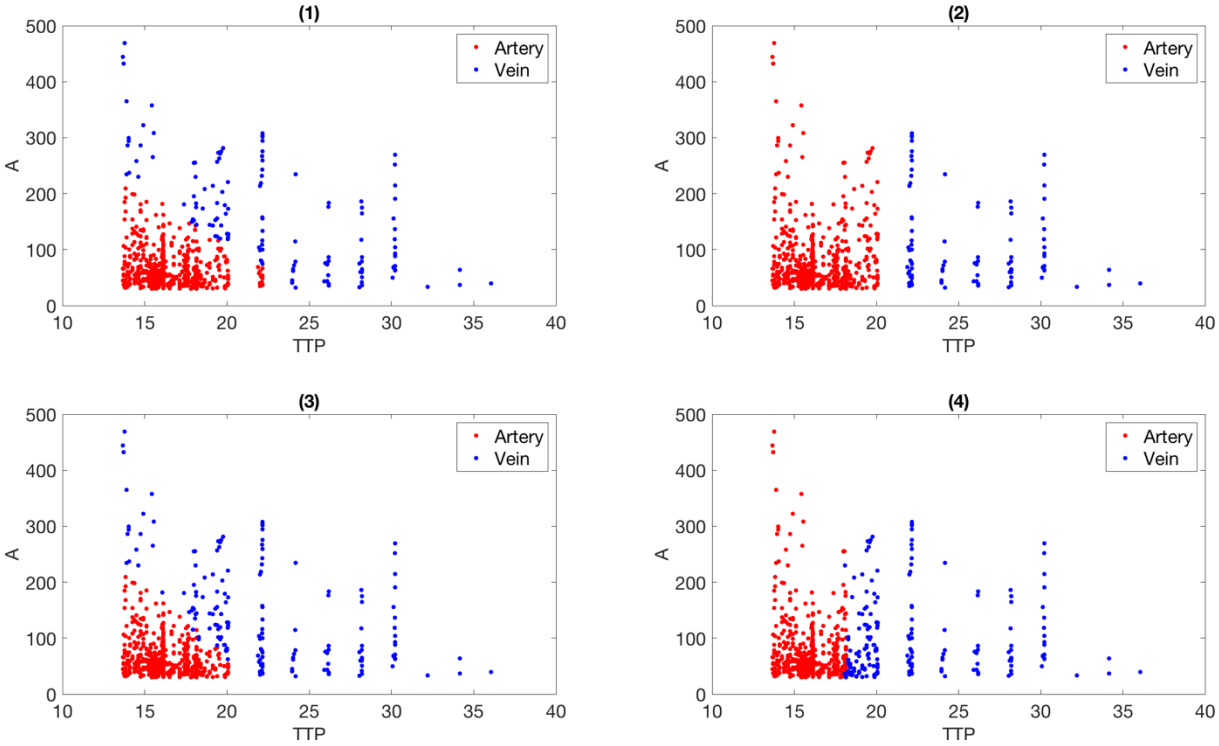

Figure 58. Clustering when different features are used to differentiate the segments. (1): TTP and attenuation (A). (2): TTP alone. (3) Parameter b from the curve fitting and attenuation (A) is used. (4): Parameter b alone.

Thus, the clustering suggests the segments for a given slice presented in Figure 59.

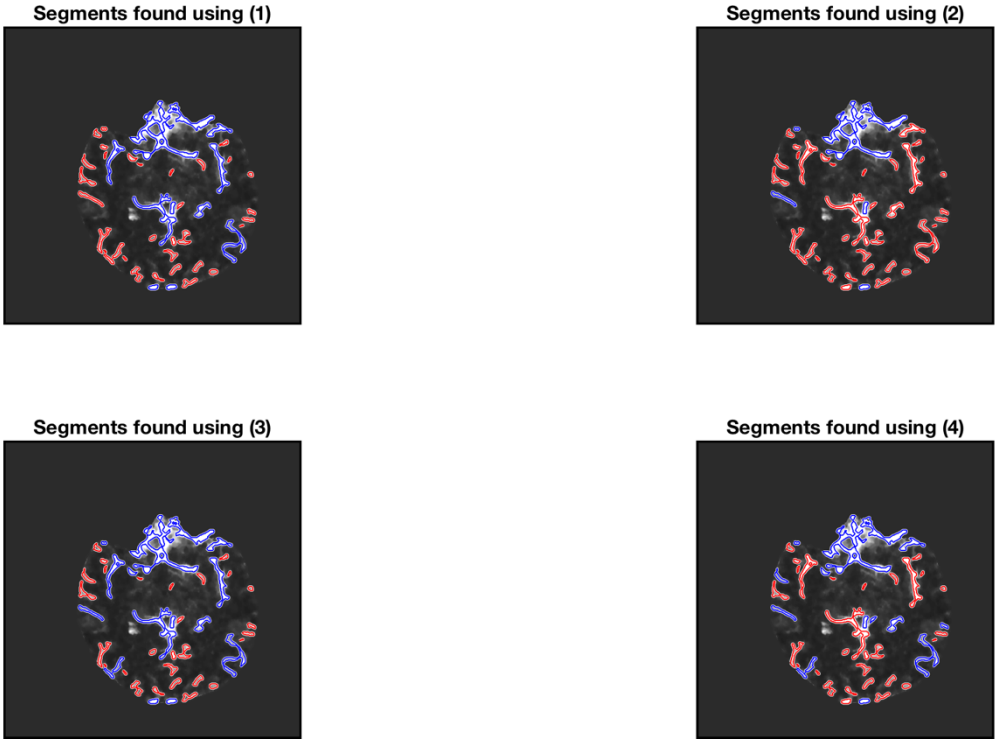

Figure 59: Segments found in a slice using different features in the clustering.

6 Discussion and conclusion

A method to segment penumbra and infarct core in parametric maps has been developed. It is possible to choose any pair of parameter combinations to determine the state of the tissue. Thus, it can be used as a framework for future experiments. It has been evaluated using combinations of TMAX and CBV or CBF. The results showed that the total size of the penumbra estimated were similar to the expert's opinion when choosing thresholds for the parameters defined in the literature. When segmenting the infarct core, the method tended to overestimate the area using rCBF<30. Choosing CBV<1.25 gave a result that was more similar to the expert's opinion.

The method provides no novel features, except for segmenting parametric maps in MATLAB if the relationship between the true parametric values in a dataset and the colors is unknown or incomplete. It is meant as an outline for something that might can be used in future research. A possibility is, for instance, to explore the use of the parameters in a classifier.

A method to automatically remove the skull and thus isolate the brain in contrast CT images of the brain have been developed. Combining edge detection by using wavelets and watershed segmentation has been shown to be a robust and promising solution to the problem. Assessing the results visually, the method successfully removes the skull, the eyes and other unwanted parts to prepare the images for further processing.

Two proposed methods for identifying vessel segments with different approaches have been developed. Both methods seem to detect the segments that are most affected by the contrast medium, i.e. the regions that probably are vessels. The segments found by the adaptive thresholding method tend to be smaller and fewer, in addition to be more disjoint compared to the cluster-based method. The overall impression is though that both are able to find approximately the same amount of the most prominent segments.

If a vessel segment is affected by the stroke, i.e. if it lies in, drains or supplies the penumbra or infarct core, this undoubtedly influences the time-density curve. This again influences the curve fitting and the derived parameters. Thus, it is prone to be removed due to too low goodness of fit, e.g. However, not doing an error checking and removal based on the time-density curves at all, will probably include segments that are not vessels. A possibility is to adjust the exclusion criteria or completely disable the curve fitting for the cluster-based segmentation. After all, the segmentation assumes that the segments are vessels based on several features describing in. Another possibility is to enable curve fitting and removal of segments only in the healthy hemisphere, as the time-density curves of vessels here will fit best to the suggested model. However, if the method is used in a clinical setting, the location of the stroke region is not necessarily known in advance.

A constraint when working with the given dataset has been the limited resolution in the z-direction, due to the slice thickness being 5 mm. Since the resolution in most of the datasets is only 13 pixels, it has not been possible to fully exploit the third spatial dimension. Thus, the

focus has been to do the segmentation in 2D. However, it is also possible to collect the features from all the slices, and then perform the clustering-based segmentation in 3D. This has been implemented, but not compared thoroughly to the 2D segmentation. The initial impression is promising, though.

An implication of the slice thickness in the given dataset is that it is harder to detect all the vessels, since a pixel actually depicts a 5 mm thick volume. If a small vessel is located deep in a slice, it may not be visible in the image, and thus not be found. Another hypothetical possibility is that what appears as a segment in the images, actually is different vessels that are close to each other in the x and y direction, but not in the z direction.

To differentiate and label the vessels with respect to type, more work needs to be conducted. If a clustering is performed, the importance and selection of each feature will have to be evaluated, as the results show.

A challenge here is the non-uniform sampling of the data. Since the time between the images is increased in the second half of the scan, this gives an increase in the distance between the data points along the time axis. The clustering interprets this as a separation, while in reality there are missing data points in between. If the contrast agent arrives in a vein just before the sample rate is reduced, it is prone to be clustered as an artery. The same goes for an artery where the contrast agent arrives after the sample rate is reduced. It will then be prone to be clustered as a vein. If a vessel is affected by the stroke, it might end up in the wrong cluster due to changes in the time-to-peak or the attenuation.

The performance of all the proposed methods will have to be evaluated in relation to ground truth. However, it is expected that both the skull removal and the vessel segmentation will have good performance.

7 References

[1] Norsk helseinformatikk, "NHI.no," [Online]. Available: https://nhi.no/sykdommer/hjernenervesystem/hjerneslag-og-blodninger/hjerneslag/?page=2.

[2] Helsedirektoratet, "Hva er hjerneslag?," [Online]. Available: https://helsenorge.no/sykdom/hjerne-og-nerver/hjerneslag/hjerneslag-arsaker.

[3] Helsedirektoratet, "Nasjonal retningslinje for behandling og rehabilitering ved hjerneslag," 2017.

[4] LHL, "Hjerneslag," [Online]. Available: https://www.lhl.no/hjertesykdom/hjerneslag/.

[5] World Health Organization, "The top 10 causes of death," [Online]. Available: http://www.who.int/mediacentre/factsheets/fs310/en/.

[6] [Online]. Available: https://helsenorge.no/sykdom/hjerne-og-nerver/hjerneslag/livet-etter-et-hjerneslag.

[7] A. Chandra, W. A. Li, C. R. Stone, X. Geng and Y. Ding, "The cerebral circulation and cerebrovascular disease I: Anatomy," vol. 3, no. 2, pp. 45-56, 2017.

[8] National Heart, Lung, and Blood Institute, "Stroke," [Online]. Available: https://www.nhlbi.nih.gov/health-topics/stroke.

[9] 1. Q. H. X. D. Q. C. K. Y. S. Z. S. Y. B. C. V. C. M. W. P. S. W. a. M. L. Yannan Yu, "Defining Core and Penumbra in Ischemic Stroke: A Voxel- and Volume-Based Analysis of Whole Brain CT Perfusion," 10 February 2016. [Online]. Available: https://www.ncbi.nlm.nih.gov/pmc/articles/PMC4748242/. [Accessed June 2018].

[10] L. Mikšík, "Basic principles of computed tomography," [Online]. Available: https://www.lf2.cuni.cz/files/page/files/2014/basic_principles_of_ct.pdf.

[11] L. L. Geyer, U. J. Schoepf, F. G. Meinel, J. W. Nance, G. Bastarrika, J. A. Leipsic, N. S. Paul, M. Rengo, A. Laghi and C. N. D. Cecco, "State of the Art: Iterative CT Reconstruction Techniques".

[12] N. Khandelwal, "CT perfusion in acute stroke," [Online]. Available: https://www.ncbi.nlm.nih.gov/pmc/articles/PMC2747454/.

[13] National Institute of Biomedical Imaging and Bioengineering, "Computed Tomography (CT)," [Online]. Available: https://www.nibib.nih.gov/science-education/science-topics/computed-tomography-ct.

[14] C. Budd and C. Mitchell, "Saving lives: the mathematics of tomography," [Online]. Available: https://plus.maths.org/content/saving-lives-mathematics-tomography.

[15] DICOM, [Online]. Available: https://www.dicomstandard.org.

[16] Innolitics, "CT Image CIOD - DICOM Standard Browser," [Online]. Available: https://dicom.innolitics.com/ciods/ct-image. [Accessed June 2018].

[17] G. N. Hounsfield, "Computed medical imaging," in *Nobel Lecture*, 1979.

[18] Innolitics, "Intercept Attribute - DICOM Standard Browser," [Online]. Available: https://dicom.innolitics.com/ciods/digital-x-ray-image/dx-image/00281052. [Accessed June 2018].

[19] "Theoretic Basis and Technical Implementations of CT Perfusion in Acute Ischemic Stroke, Part 1: Theoretic Basis".*American Journal of Neuroradiology.*

[20] K. Kudo, M. Sasaki, L. Ø. S. Christensen, I. Uwano, M. Suzuki, K. Ogasawara, H. Shirato and A. Ogawa, "Susceptibility of Tmax to tracer delay on perfusion analysis: quantitative evaluation of various deconvolution algorithms using digital phantoms," *The Journal of Cerebral Blood Flow & Metabolism,* pp. 908-912, March 2011.

[21] "Evaluation of CT Perfusion in the Setting of Cerebral Ischemia: Patterns and Pitfalls".

[22] L. Lin, A. Bivard and M. Parsons, "Perfusion Patterns of Ischemic Stroke on Computed Tomography Perfusion," [Online]. Available: https://www.ncbi.nlm.nih.gov/pmc/articles/PMC3859000/.

[23] C. Kirbas and F. Quek, "A Review of Vessel Extraction Techniques and Algorithms," 2003.

[24] F. Bukenya, A. Kiweewa and L. Bai, "A Review of Vessel Segmentation Techniques," in *International Conference on Computer Vision and Image analysis*, 2017.

[25] M. Meijs, A. Patel, S. C. v. d. Leemput, M. Prokop, E. J. v. Dijk, F.-E. d. Leeuw, F. J. A. Meijer, B. v. Ginneken and R. Manniesing, "Robust Segmentation of the Full Cerebral Vasculature in 4D CT of Suspected Stroke Patients," *Scientific Reports,* vol. 7, no. 7, 15 Nowember 2017.

[26] L. Breimann, "Random forests," *Machine Learning,* no. 45, pp. 5-32, 2001.

[27] B. Zitová and J. Flusser, "Image registration methods: a survey," *Image and Vision Computing,* no. 21, pp. 977-1000, September 2003.

[28] J. Cross, "Computed Tomography in Neurology," *ACNR,* vol. 8, no. 5, November/December 2008.

[29] B. S. Reddy and B. N. Chatterji, "An FFT-Based Technique for Translation, Rotation, and Scale-Invariant Image Registration," *IEEE Transactions on Image Processing,* vol. 5, no. 8, August 1996.

[30] S. Eddins, "Watershed transform question from tech support," [Online]. Available: https://blogs.mathworks.com/steve/2013/11/19/watershed-transform-question-from-tech-support/#view_comments.

[31] Y. Takashimizu and M. Iiyoshi, "New parameter of roundness R: circularity corrected by aspect ratio," *Progress in Earth and Planetary Science,* vol. 3, no. 2, 2016.

[32] C. Tomasi and R. Manduchi, "Bilateral Filtering for Gray and Color Images," in *IEEE International Conference on Computer Vision*, 1998.

[33] A. F. Frangi, W. J. Niessen, K. L. Vincken and M. A. Viergever, "Multiscale vessel enhancement filtering," in *International Conference on Medical Image Computing and Computer-Assisted Intervention*, 1998.

[34] J. Delpiano, "Fast mutual information of two images or signals," [Online]. Available: https://se.mathworks.com/matlabcentral/fileexchange/13289-fast-mutual-information-of-two-images-or-signals.

[35] S. Shetty and M. Lev, in *Acute Ischemic Stroke: Imaging and Intervention*, R. González, J. Hirsch, M. Lev, P. Schaefer and L. Schwamm, Eds., 2011.

[36] A. Fieselmann, M. Kowarschik, A. Ganguly, J. Hornegger and R. Fahrig, "Deconvolution-Based CT and MR Brain Perfusion Measurement: Theoretical Model Revisited and Practical Implementation Details," *International Journal of Biomedical Imaging,* 2011.

[37] T. Bäck, C. Foussette and P. Krause, "Evolution Strategies," in *Contemporary Evolution Strategies*, Springer, 2013.

Attachment A: Matlab code

matlab code.7z attached